UC San Diego
UC San Diego Electronic Theses and Dissertations

Title
The kinetics of bacterial growth transitions

Permalink
https://escholarship.org/uc/item/4pk7r12q

Author
Erickson, David William

Publication Date
2014

Peer reviewed|Thesis/dissertation

UNIVERSITY OF CALIFORNIA, SAN DIEGO

The kinetics of bacterial growth transitions

A dissertation submitted in partial satisfaction of the
requirements for the degree
Doctor of Philosophy

in

Physics (Biophysics)

by

David William Erickson

Committee in charge:

Terence T. Hwa, Chair
Jeff M. Hasty
William F. Loomis, Jr.
Wouter-Jan Rappel
Douglas E. Smith

2014

The dissertation of David William Erickson is approved, and it is acceptable in quality and form for publication on microfilm and electronically:

_____

_____

_____

_____

_____

Chair

University of California, San Diego

2014

DEDICATION

To my family.

TABLE OF CONTENTS

LIST OF FIGURES

LIST OF TABLES

ACKNOWLEDGEMENTS

First I would like to thank my family for their continuous support and love. Thank you to my father Mark who always made sure that I was keeping on top of my studies and pushed me to be independent from a young age. Thank you to my mother Michelle who instilled in me an openness to the world and ideas and who reminds me to slow down and enjoy the present. I thank my sister Mary for putting up with me at my worst, while always reminding me of my best. A very special thank you to my grandparents Bill and Dorothy Erickson, who provided unconditional love in a way that I think only grandparents are able to. You both always made sure that I knew the value of education. Nana, I have always felt your love and support and I know that you would do anything for me. Papa, you always made me feel special and taught me the value of hard work and social responsibility.

I would like to thank everybody in the Hwa group for their help and support. Thanks to Professor Terry Hwa for mentoring me. You have shown me how to be rigorous and the importance of considering as many perspectives as you can. Thank you for the personal attention on every detail. I have learned much from you. Thank you Zhongge Zhang, Tom Kuhlman, Matt Scott, and Carl Gunderson for teaching me the basics of molecular biology and bacterial growth. I would like to acknowledge Dr. Sheng (Tony) Hui. Your encyclopedic knowledge and the discussions that we've had have been more valuable than you know. Thank you Dr. Jonas Cremer for great discussions. You were always happy to discuss specifics and generalities of science. You have been a great sounding board and discussions with you have been scientifically and personally enriching.

I would like to acknowledge Professor Uli Gerland for piquing my interest in the kinetics of bacterial growth transitions and getting the subject of this dissertation started. I would like to acknowledge Severin Schink for all of his contributions to this project.

I would like to acknowledge my committee for providing valuable comments about my work.

With permission from the coauthors, all chapters of this dissertation contain work from a manuscript that is in preparation with the working title "A quantitative

theory for the kinetics of bacterial growth transition" 2014, D. W. Erickson, S. Schink, U. Gerland, and T. Hwa.

VITA

2006	B. Sc. in Physics and Mathematics *summa cum laude*, Virginia Tech
2014	Ph. D. in Physics (Biophysics), University of California, San Diego

PUBLICATIONS

D. W. Erickson, S. Schink, U. Gerland, and T. Hwa. A quantitative theory for the kinetics of bacterial growth transition. In preparation.

S. Hui, J. M. Silverman, **D. W. Erickson**, J. Wang, T. Hwa, and J. R. Williamson. Metabolic partitioning of bacterial proteome as a principle of global regulation of gene expression. In submission.

R. Hermsen, **D. W. Erickson**, and T. Hwa. Speed, sensitivity, and bistability in auto-activating signaling circuits. *PLoS Comp. Bio.* 7, e1002265 (2011)

Y. Hao, Z. Zhang, **D. W. Erickson**, M. Huang, Y. Huang, J. Li, T. Hwa, and H. Shi. Quantifying the sequence-function relation in gene silencing by bacterial small RNAs. *PNAS* 108, 1247312478 (2011)

ABSTRACT OF THE DISSERTATION

The kinetics of bacterial growth transitions

by

David William Erickson

Doctor of Philosophy in Physics (Biophysics)

University of California, San Diego, 2014

Professor Terence T. Hwa, Chair

Bacteria in changing environments must constantly adapt to grow and survive. The adaptive response to change can be extremely complex, as it depends not only on the current conditions, but also on the history of the cell over many generations. For this reason, most of our understanding of bacterial physiology comes from so-called steady state growth, where cultures are grown in static environments for a long time. As a first step toward understanding the kinetics of adaptation, we build on the foundation of steady-state growth and study transitions between two well-defined steady states of *E. coli*.

We first focus on carbon upshifts, in which cells growing in steady state are supplemented with a better carbon source and transition to a new steady state with faster growth. We observe that the response of growth rate has multiple timescales and

occurs over the course of several generations. The rate of biomass accumulation (*i.e.* flux), on the other hand, reaches its final behavior much more quickly. We develop a model that quantitatively reproduces these kinetics using only empirical observations of ribosome and catabolic enzyme synthesis in steady state and the known topology of regulatory interactions. The model is solved analytically and has only a single free parameter that captures the initial influx of the added carbon. We predicted that if this initial flux is high enough the growth rate can transiently exceed its steady state value for several hours; this is verified by synthetically titrating carbon transport enzymes. We also studied carbon downshifts, in which cells growing on a combination of two carbon sources deplete one of them and transition to slower steady state growth on only a single carbon source. We observe that the growth rate recovers more quickly than for upshifts, but the growth kinetics are also quantitatively captured by our model. We are able to reproduce surprising and counterintuitive kinetics of growth transitions with a conceptually simple model. The success of our approach demonstrates the power of empirical characterizations to quantitatively capture biological phenomena.

Chapter 1

Introduction and background

1.1 Introduction

In nature bacteria must constantly adapt to environmental changes in order to grow and survive. Indeed, even in industrial bioreactors it is difficult to maintain an optimal homogeneous growth environment and metabolic shifts are common [1]. Understanding how bacteria adapt to the changes in their environment is a major challenge of bacterial physiology and systems biology [2].

Here we study the kinetics of *Escherichia coli* throughout growth transitions. We begin in this chapter by reviewing important observations about bacterial growth in constant environments. We then briefly discuss the commonly studied types of growth transitions and define the growth transitions that we focus on here. In Chapter 2 we present observations of the kinetics of mass accumulation throughout carbon upshift transitions. In Chapter 3 we derive a simple analytical model of carbon upshift using the observations from Chapter 1 and insights from the general observations made in Chapter 2. In Chapter 4 we compare the model to experimental observations and find good agreement. In Chapter 5 we extend the simple model to carbon downshift transitions and compare to observations. In Chapter 6 we summarize general lessons from this study and remaining questions and future directions.

1.2 Steady state balanced growth

Steady state, or balanced, growth is defined as the condition in which all cell constituents increase by the same factor during the same time interval [3]. Bacteria maintained in a proper constant environment for a long time grow exponentially and reach steady state. The steady state growth condition is maintained indefinitely as long as the environment is unchanged. Steady state growth provides a well-defined, reproducible condition for studying bacterial physiology [4].

In steady state growth, the exponential rate of growth of the culture (the "growth rate") rate is an important quantity. By definition, in steady state growth each cellular constituent (X) increases with the steady state growth rate (λ^*)

$$\frac{dX}{dt} = \lambda^* X. \tag{1.1}$$

Here, and throughout this document, we use asterisks (*) to denote intrinsic quantities observed in steady state balanced growth. The growth rate quantifies the ability of the bacteria to grow in the prescribed environment and can be quantified accurately, easily, and reproducibly [5]. Remarkably, despite the immense complexity of underlying regulatory networks, the macromolecular composition of the bacterial cell is found to depend primarily on the growth rate of bacteria in steady state growth, largely independent of the specific nutrients in the growth medium [6] [7] [8] [9].

1.2.1 Ribosome line

Protein synthesis machinery (*i.e.* ribosomes and affiliated factors) plays a central role in microbial growth. To keep up with the need for high rates of protein synthesis at fast steady state growth rates, cells have increased ribosome content [6] [10] [11] [12]. For *E. coli* in steady state exponential growth with growth rate modulated by the nutritional quality of the medium, the RNA/protein ratio is linearly correlated with the growth rate λ^* [11] [13] [9]. For example, in Fig. 1.1 we plot the RNA/protein data from Table S10 of [14] with growth rate modulated by carbon source. The RNA/protein ratio is well established as a proxy for ribosome content [6] [9]. Thus in steady state there is a linear
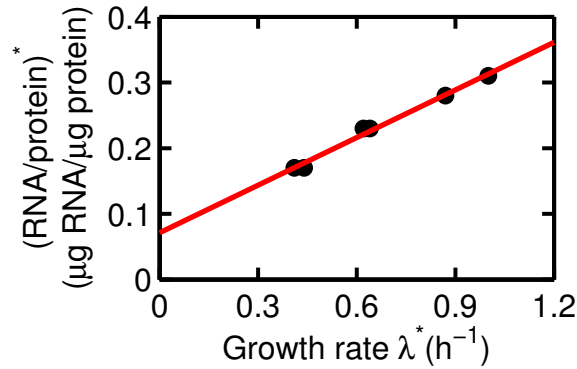
Figure 1.1: Linear correlation between growth rate and RNA/protein. Growth rate of wild-type *E. coli* NCM3722 is varied by nutrient quality during batch culture growth in 37°C with good aeration. Total RNA and total protein amounts are quantified and the ratio RNA/protein is linearly correlated with growth rate. Black points are data. Red line is a linear fit to the data shown.

relationship between the growth rate and the ribosomal mass fraction

$$\phi_R^* = \phi_{R,\min} + \lambda^*/\gamma_{\max} \tag{1.2}$$

with

$$\phi_R \equiv M_R/M, \tag{1.3}$$

where M_R is the total mass of ribosomal proteins together with their affiliates, including all the initiation factors, elongation factors, tRNA synthases, etc., and M is total protein mass. The line is completely determined by the constants describing the vertical intercept ($\phi_{R,\min}$) and the slope ($1/\gamma_{\max}$). We refer to the linear relationship between ribosomal mass fraction and growth rate as "the ribosome line".

The increasing fraction of total protein devoted to ribosomes can be rationalized by considering constraints on the cell. To achieve faster growth the cell must produce protein at a faster rate. All protein synthesis is a result of the activity of ribosomes. Thus the cell needs amount of ribosomes at faster growth. The cell could maintain a large ribosomal mass fraction even at slow growth, but this would come at the expense of other (presumably more useful) proteins.

1.2.2 Translational activity

In steady state growth the rate of protein synthesis is equal to the rate of growth. Since ribosomes catalyze protein synthesis, the demand for ribosome activity depends intimately on the growth rate. The cell can meet the demand for protein synthesis by changing the amount of ribosomes and by adjusting the catalytic rate of the ribosome. We already showed above that in steady state the ribosome abundance is a linearly increasing function of the growth rate. In this section we will discuss the catalytic rate of the ribosome.

We define "translational activity" (γ) as the protein synthesis rate per ribosome mass

$$\gamma \equiv \left(\frac{dM}{dt} \right) / M_R. \tag{1.4}$$

Here we do not distinguish between active and inactive riboomes; γ is the average activity of all ribosomes. In steady state, protein synthesis rate is related to growth rate in accordance with Eq. (1.1) and we can express the translational activity in terms of the ribosomal mass fraction (defined in Eqs.. (1.3) and (1.4), respectively)

$$\gamma^* = \lambda^* / \phi_R^*. \tag{1.5}$$

Using Eq. (1.5) we can calculate the translational activity purely from the growth rate and the ribosomal mass fraction in steady state. We use the growth rate dependence of the ribosomal mass fraction (Eq. (1.2)) to calculate the translational activity as a function of steady state growth rate

$$\gamma^* = \frac{\lambda^*}{\phi_{R,\min} + \lambda^* / \gamma_{\max}}. \tag{1.6}$$

The translational activity is found to be a Michaelis-Menten function of the steady state growth rate.

The dependence of translation speed on growth rate in steady state is well known [15] [16] [17] [11] [15]. The growth rate dependence of the translation speed is well described by a Michaelis-Menten function and was recently found to be consistent with the coregulation of ribosome- and tRNA-affiliated proteins [18].
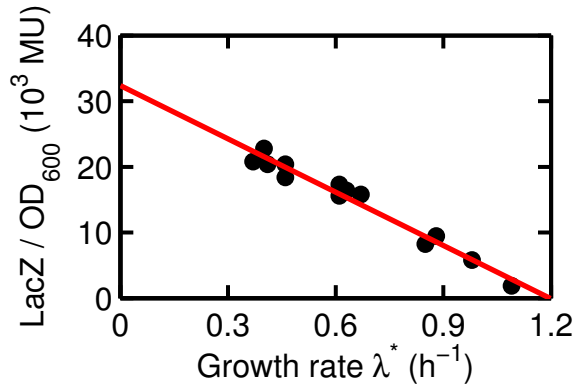
Figure 1.2: Linear correlation between growth rate and catabolic protein abundance.

1.2.3   Catabolic line

We have thus far explored the growth rate dependence of the abundance and activity of the protein synthesis machinery in *E. coli*. Of course, the translation machinery requires amino acid substrates to make proteins. In this section we will explore the growth rate dependence of the carbon influx machinery required to provide the building blocks for protein synthesis.

Cyclic AMP (cAMP) has a global regulatory role in *E. coli* and is required for the expression of many catabolic enzymes [19] [20]. The synthesis of cAMP is inhibited by glucose uptake via the phosphotransferase system [21] [22]. *E. coli* grown on PTS-independent carbon sources has also showed reduced cAMP levels [23] [24] [25]. Recently it was shown that in steady state the mass fraction of cAMP-dependent catabolic proteins correlates linearly with growth rate when *E. coli* is grown in minimal medium batch culture with different carbon sources [14]. We replot the data from Table S1 of [14] in Fig. 1.2. The Lac repressor (LacI) was deactivated using isopropyl-β-D-thiogalactopyranoside (IPTG) to characterize the cAMP-dependent expression level [26]. We note that OD600 is roughly proportional to total protein independent of nutrient conditions (see Fig. S14 in [14]) so that the y-axis of Fig. 1.2 is proportional to the mass fraction of LacZ. Then

$$\phi_{Cj}^* = h_{Cj}(1 - \lambda^*/\lambda_C) \tag{1.7}$$

where

$$\phi_{Cj}^{*} \equiv M_{Cj}/M \tag{1.8}$$

is the mass fraction of the catabolic protein M_{Cj}. The constant h_{Cj} is the y-intercept and is specific to each catabolic protein. The constant λ_C is the x-intercept and is shared by all proteins. We refer to the linear relationship between catabolic mass fraction and steady state growth rate as "the catabolic line".

1.2.4 Growth rate addition

Bacteria cultured in the presence of two carbon sources can either consume them both simultaneously (simultaneous usage) or consume only one while suppressing metabolism of the other (hierarchical usage). Here we discuss simultaneous carbon usage. We show that the steady state growth rate of *E. coli* on the combination of carbon sources can be predicted from the knowledge of the steady state growth rates on the individual carbon sources.

For saturating concentrations of carbon source Cj its influx is

$$J_{Cj} = k_{Cj}M_{Cj}. \tag{1.9}$$

k_{Cj} is the catabolic rate constant. M_{Cj} is the mass of the rate-limiting catabolic enzyme for the carbon source Cj. In the simplest case of simultaneous carbon usage the total carbon flux is the sum of the individual carbon fluxes. Then the total carbon flux J_C for *E. coli* cultured in the presence of two carbon sources ($C1$ and $C2$) is

$$J_C = k_{C1}M_{C1} + k_{C2}M_{C2}. \tag{1.10}$$

The carbon efficiency relates carbon flux to protein flux

$$c_0 \equiv \frac{dM}{dt}/J_C. \tag{1.11}$$

It was recently observed that the carbon efficiency c_0 is constant and thus carbon flux is proportional to protein synthesis flux (Table S8 in [27]). We use the steady state condition Eq. (1.1) for total protein mass to find a relationship between carbon flux and

the steady state growth rate

$$\lambda^* = c_0 \frac{J_C}{M}. \tag{1.12}$$

The catabolic line discussed in Sec. 1.2.3 relating the expression of catabolic enzymes to the steady state growth rate in minimal medium supplemented with different carbon sources is also observed for growth on multiple carbon sources. Thus the expression of the catabolic proteins is captured by the catabolic line Eq. (1.7) ($\phi_{Cj}^* = h_{Cj}(1 - \lambda^*/\lambda_C)$).

The mass fraction of catabolic proteins is related to the steady state growth rate by the catabolic line Eq. (1.7). The mass fraction of the catabolic proteins, in turn, determine the total carbon flux by flux addition Eq. (1.10). The resulting total carbon flux is related to the growth rate via the carbon efficiency by Eq. (1.12). Combining these three observations reveals that for growth on two carbon sources (with steady state growth rate λ_{12}^*)

$$\frac{\lambda_{12}^*}{\lambda_C - \lambda_{12}^*} = c_0 \left(k_{C1} h_{C1} + k_{C2} h_{C2} \right). \tag{1.13}$$

For growth on a single carbon source Cj with growth rate λ_j^*, the same calculation yields

$$\frac{\lambda_j^*}{\lambda_C - \lambda_j^*} = c_0 \left(k_{Cj} h_{Cj} \right). \tag{1.14}$$

Substituting Eq. (1.14) into Eq. (1.13) we find

$$\frac{\lambda_{12}^*}{\lambda_C - \lambda_{12}^*} = \frac{\lambda_1^*}{\lambda_C - \lambda_1^*} + \frac{\lambda_2^*}{\lambda_C - \lambda_2^*}. \tag{1.15}$$

The growth rate on two simultaneously used carbon sources can be quantitatively predicted solely in terms of the growth rates on the individual carbon sources and the constant phenomenological parameter λ_C. The validity of this relation has been verified for growth on simultaneously used carbon sources in steady state [28].

Our model for the kinetics of bacterial growth transitions relies on the same equations as this two carbon growth rate formula derivation. The fact that Eq. (1.15) is quantitatively verified provides a measure of confidence in the validity of Equations (1.7), (1.10) and (1.12) and their applicability.

1.3 Dynamic nutrient environments

Thus far we have described observations about the growth of *E. coli* in steady state exponential growth. Studying steady state growth is unparalleled as a tool to study bacterial physiology because it provides a well-defined and reproducible condition. But in nature the availability of nutrients changes in time. Bacteria must adapt to the changing environment in order to grow and survive. Indeed, bacterial fitness is dependent on how they adapt to changing conditions. Here we will investigate the kinetics of biomass accumulation in changing nutrient environments.

In order to have a chance to understand physiology in dynamic nutrient environments we will study well-defined and reproducible transitions. Thus we seek a dynamic nutrient environment with initial and final conditions in steady state exponential growth.

1.3.1 Diauxie and carbon downshift

Diauxie, the canonical growth transition, is the biphasic growth pattern observed when an organism is grown on a pair of carbon sources [29]. The culture exhibits two periods of exponential growth separated by a lag period. An example growth curve for a diauxie transition is shown in Figure 1.3. We here distinguish two different kinds of diauxie: hard diauxie and soft diauxie (or '"carbon downshift").

Hard diauxie is characterized by strict inhibition of the metabolism of one of the carbon sources in the first growth phase. Each period of exponential growth then corresponds to exclusive utilization of a single carbon source [30]. The glucose-glycerol diauxie growth curve in Figure 1.3 is an example of hard diauxie. Initially glucose and glycerol are both present. $OD600$ increases exponentially and glucose, the preferred carbon source, is consumed. Once glucose is exhausted a characteristic lag is observed as the culture adapts to the new nutrient condition (growth on glycerol as the sole carbon source). Eventually the culture reaches a new steady state growth condition.

Soft diauxie (or "carbon downshift") is characterized by simultaneous usage of both carbon sources in the initial growth phase. $OD600$ increases exponentially during this phase until one of the carbon sources is depleted. The disappearance of this carbon source results in a sudden decrease in the total cellular carbon influx. The characteristic
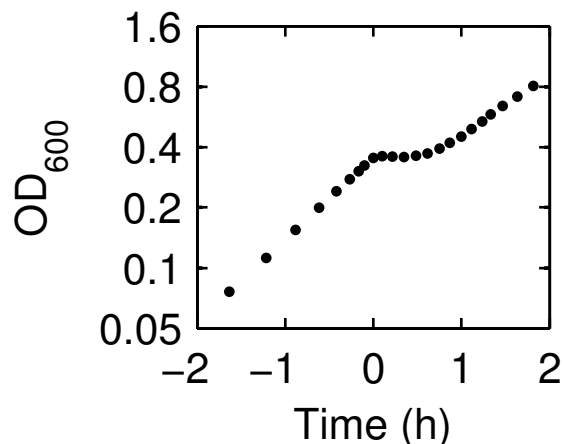
Figure 1.3: Glucose-glycerol diauxie. Wild-type *E. coli* NCM3722 is grown at 37°C in minimal medium with glucose and glycerol. The growth curve exhibits the characteristic diauxie lag. The data is reported in Table 7.3

diauxic lag occurs as the cells adapt to the new environment (growth on a single carbon source).

In diauxie the initial and final growth states are well-defined (steady state balanced growth). Diauxie is also the best known and best studied example of a dynamic nutrient environment. However, *diauxie is a complicated kinetic process*. The culture is initially in a steady state, but once one carbon source is exhausted the cells are suddenly in a carbon-poor condition. As the cells adapt to the new environment they metabolize the new carbon source and leave the carbon-poor state as they transition to their final steady state. So in diauxie the culture experiences two transitions: first a drop in carbon quality as one carbon source is exhausted and then an increase in carbon quality as the cell adjusts its metabolism. In addition, the intermediate carbon-poor state is very poorly understood. We note here that in carbon downshift the intermediate carbon-poor state is less severe than for hard diauxie. This relieves one of the difficulties of understanding the diauxie growth transition. In Chapter 5 we will explore carbon downshifts, but we first seek a simpler dynamic growth environment before expanding to more complicated transitions.

1.3.2 Carbon upshift

We deem the dynamic nutrient condition at the core of this work "carbon upshift". *E. coli* is cultured at 37°C in minimal medium with a single carbon source. During steady state exponential growth a second carbon source is added to the medium and both carbon sources are in surplus for the rest of the experiment. The second carbon source allows faster growth so that the culture transitions from slower to faster growth.

Carbon upshifts are simple dynamic nutrient environments. They involve only a single transition from one steady state growth condition to another. All nutrients are always in surplus so that there are no intermediate nutrient-poor states. The transition from slower to faster growth results from the addition of just a single compound. In the literature it is common to add a cocktail of many compounds [31], which significantly complicates understanding. The simplicity of carbon upshifts provides a minimal model system for the study of the kinetics of mass accumulation in dynamic nutrient environments.

Aside from being a nice model system for the study of dynamic nutrient environments, carbon upshifts have practical importance. Carbon upshifts should be ubiquitous in nature and understanding how bacteria adapt has clear implications for fitness; faster adaptation is fitter, all other things being equal.

1.4   Acknowledgments

With permission from the coauthors, all chapters of this dissertation contain work from a manuscript that is in preparation with the working title "A quantitative theory for the kinetics of bacterial growth transition" 2014, D. W. Erickson, S. Schink, U. Gerland, and T. Hwa.

Chapter 2

Kinetics of mass accumulation throughout carbon upshift

2.1 Introduction

In this chapter I describe general observations about the kinetics of mass accumulation throughout carbon upshift. I first describe our experimental setup.

2.2 Flowcell

To study the kinetics of mass accumulation requires precise, accurate observations with good temporal resolution for many hours. To meet these requirements we constructed the experimental setup in Fig. 2.1 to measure OD600 continuously. *E. coli* is cultured in a shaking Erlenmeyer flask. A peristaltic pump is used to pump the culture from the flask to a flowcell cuvette and back to the flask. The OD600 of the culture in the cuvette is measured continuously. The entire device is kept in an incubator at 37°C.

A typical growth curve for wild-type *E. coli* K-12 in steady state balanced growth in the flowcell device is plotted in Fig. 2.2. The OD600 is exponential in time (solid black points). The data points are barely visible behind the fitted exponential curve (red line). The observed growth rate $(0.89\,\mathrm{h}^{-1})$ is comparable to batch culture observations $(\lambda_{glucose} = 0.88\,\mathrm{h}^{-1})$. We generally observe the same growth rate in the flowcell device as in batch culture, providing confidence that the experimental setup is not influencing
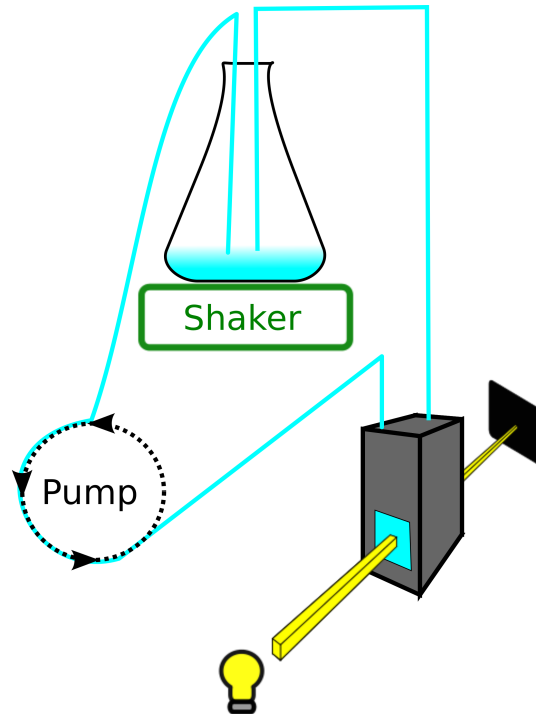
Figure 2.1: A cartoon of the flowcell device setup. The entire setup is contained in an incubator held at 37°C. *E. coli* is cultured in a shaking (250rpm) Erlenmeyer flask. A peristaltic pump is used to pump the culture from the flask to a flowcell cuvette and back. While in the flowcell cuvette a spectrophotometer measures OD600.

our results.

2.3 OD600 throughout carbon upshift

A typical growth curve throughout carbon upshift is shown in Fig. 2.3. We define time relative to the time at which the new carbon source is added so that $t = 0$ is the moment of addition. Before upshift ($t < 0$) the culture is in steady state exponential growth on the single carbon source mannose and thus follows the exponential curve plotted in red. At $t = 0$ the second carbon source lactose is added to the culture so that for $t > 0$ the culture adjusts to a new, faster steady state exponential growth rate and thus increases faster than the red curve.
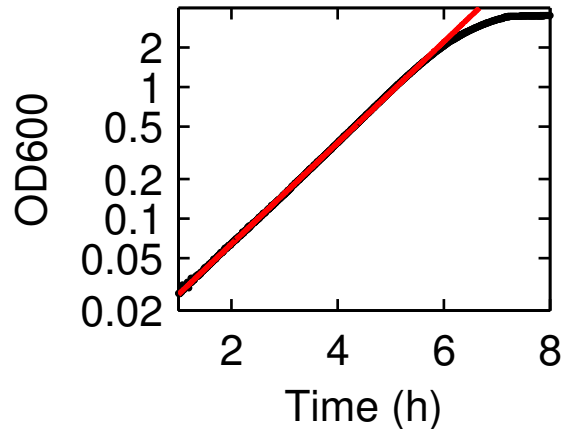
Figure 2.2: Steady state growth on glucose in the flowcell device. NCM3722 in steady state balanced growth on glucose in the flowcell device.

2.4 Growth rate relaxes on a long timescale

The raw growth curve does not nicely convey how the bacteria adjust to the new nutrient condition. Typically the steady state growth rate, defined as the slope of the logarithm of biomass, is used to quantify the rate of mass accumulation. Here, we generalize the growth rate concept to kinetic situations and define the instantaneous growth rate as the local slope of the logarithm of total protein mass (M)

$$\lambda \equiv \frac{d}{dt} ln[M] \tag{2.1}$$

We take OD600 as a measure of total protein and note that OD600 is a good proxy for total protein independent of nutrient conditions (see Fig. S14 in [14]). Growth rate as defined here is a useful quantity because it captures the exponential rate of growth. In steady state, growth is exponential and thus growth rate is constant. Carbon upshift experiments start with a culture in steady state balanced growth with initial growth rate (λ_i) and add a new carbon source and the culture adjusts to a new, faster steady state growth rate (λ_f). Thus a plot of growth rate is constant before upshift and eventually reaches a new, higher constant value.

A typical plot of growth rate throughout carbon upshift is shown in Fig. 2.4. Each point is the growth rate calculated using Eq. (2.1) over a rolling 2 minute time window. The known steady state initial and final growth rates are shown (red and
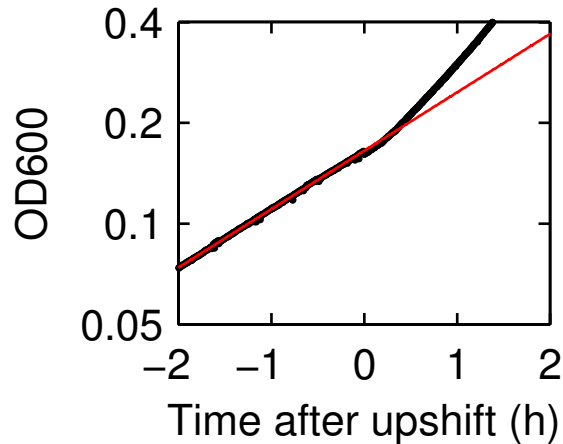
Figure 2.3: Growth curve for mannose add lactose upshift in the flowcell device. Growth curve for wild-type NCM3722 cells for mannose add lactose upshift. Black points are OD600 data. The red curve is an exponential fit to the portion of the growth curve on mannose alone. The observed growth rate $(0.4\,\mathrm{h}^{-1})$ is the same as batch culture observations.

green, respectively). Before carbon upshift the culture is in balanced growth and the instantaneous growth rate is constant in time with the known initial steady state growth rate $\lambda_i = 0.4\,\mathrm{h}^{-1}$. After the first $\approx$30min the growth rate of the culture has increased halfway to the final growth rate. Suddenly the growth rate begins increasing with a slower timescale and it takes more than an hour to increase half of the remaining growth rate difference. Surprisingly, growth rate is still increasing an hour and a half after carbon upshift. This long timescale behavior is not specific to this carbon upshift, as will be seen later. Sufficiently long after carbon upshift, the growth rate must reach the constant final steady state growth rate λ_f.

To observe that the cultures eventually reach the final steady state exponential growth rate requires observation for much longer times. To accomplish this we must serially dilute the culture throughout growth to prevent saturation. Figure 2.5 shows the growth rate of a succinate add gluconate culture over much longer times (up to 5 h) after upshift. At the moment of upshift, growth rate increases about halfway from the initial steady state growth rate $(\lambda_i = 0.45\,\mathrm{h}^{-1})$ to the final steady state growth rate $(\lambda_f = 0.88\,\mathrm{h}^{-1})$. After this growth rate continues to relax but with a much slower timescale. Growth rate does not reach the final steady state growth rate until about 2 h

Figure 2.4: Growth rate for mannose add lactose upshift in the flowcell device. Growth rate plotted versus time for wild-type NCM3722 cells for mannose add lactose upshift. Black points are growth rate data. The red curve shows the steady state growth rate for cultures on mannose alone. The green curve shows the steady state growth rate for cultures on the combination of mannose and lactose.

after upshift. Growth rate remains fixed at the final steady state growth rate for the indefinite future.

2.5 Flux relaxes on a fast timescale

We have thus far observed OD, which reflects the amount of biomass, and observed that it does not give much insight into the kinetics of mass accumulation throughout carbon upshift. We also observed growth rate, which measures the rate of exponential accumulation of biomass, and found that after carbon upshift, growth rate increases towards its final value quickly at first and then slows down and reaches the constant final growth rate only after several doublings.

To further probe the kinetics of mass accumulation we look directly at the rate of biomass accumulation. The protein synthesis flux, or flux for short, is the rate of accumulation of total protein mass

$$J \equiv \frac{d}{dt}[M].$$
(2.2)

We again note that we take OD600 as a measure of total protein (OD600 is a good proxy

Figure 2.5: Long time growth rate for succinate add gluconate upshift. Wild-type NCM3722 cells were grown in minimal medium at 37°C with 1 mM IPTG and 0.4% succinate as the sole carbon source. At time zero gluconate was added to a final concentration of 20 mM. Culture saturation was avoided by serial dilution into a fresh, identical culture. The original culture was grown from -2.5h to 2h, the second culture from 1.3h to 3.3h, and the final culture from 3h to 4.7h. The raw OD600 data is reported in Table 7.4. Black points are growth rate calculated from two consecutive OD600 measurements. The red dashed line indicates the steady state growth rate of the initial culture before upshift. The green solid line indicates the steady state growth rate of the culture after upshift.

for total protein independent of nutrient conditions; see Fig. S14 in [14]).

In steady state, protein mass increases exponentially in time with rate equal to the growth rate. Thus the protein synthesis flux, which is the production rate of protein, also increases exponentially in time with rate equal to the growth rate. In carbon upshift experiments the culture is initially in steady state growth and thus the flux grows exponentially with the initial growth rate. Eventually, the culture reaches a new, faster steady state growth rate and thus the flux also grows exponentially in time with the same rate.

A typical plot of flux throughout carbon upshift is shown in Fig. 2.6. Each point is flux calculated using Eq. (2.2) over a rolling 2 minute time window. The known steady state flux curves for the initial and final steady states are shown (red and green, respectively). Before carbon upshift, the culture is in steady state growth and the flux grows exponentially with rate equal to the initial growth rate $\lambda_i = 0.4 \, \mathrm{h}^{-1}$. During the first $\approx$30min the flux increases very quickly. Next the flux increases exponentially in
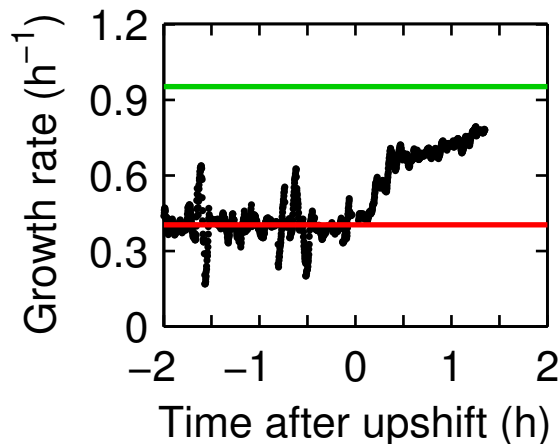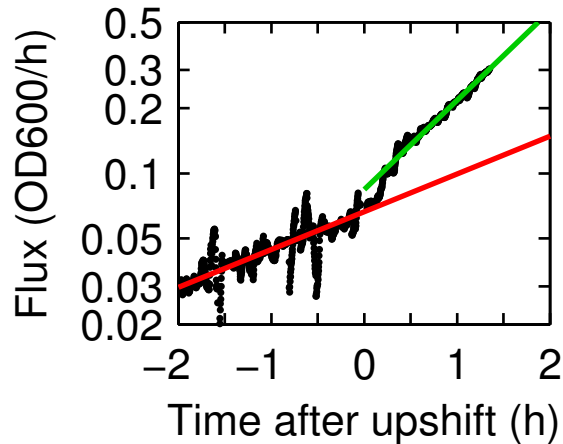
Figure 2.6: Flux for mannose add lactose upshift in the flowcell device. Flux plotted versus time for wild-type NCM3722 cells for mannose add lactose upshift. Black points are growth rate data. The red curve shows the flux for steady state growth on mannose alone. The green curve shows the flux for cultures growing in steady state on the combination of mannose and lactose.

time with rate equal to the final growth rate λ_f =0.95 h^{-1}. The flux continues to grow exponentially with rate λ_f indefinitely as long as the proper conditions are maintained. Thus, unlike growth rate, flux reaches its final steady state behavior quickly ($\approx$30min) after carbon upshift. We will see later that this quick relaxation of flux to the final steady state behavior is general.

We wish to observe cultures for long times after upshift. To accomplish this we must serially dilute the culture throughout growth to prevent saturation. Figure 2.7 shows the growth rate of a succinate add gluconate culture over much longer times (up to 5 h) after upshift. Before upshift the flux grows with exponential rate equal to the initial steady state growth rate (λ_i =0.45 h^{-1}). At the moment of upshift, flux increases very quickly so that it appears to have a jump within the time precision of our batch culture measurements. Beginning soon afterwards, flux increases exponentially with rate equal to the final steady state growth rate (λ_f =0.88 h^{-1}). This continues for the duration of observation.

The kinetics of flux throughout carbon upshift is relatively simple. Flux increases exponentially before upshift because the culture is in steady state. Flux increases in a nontrivial manner just after carbon upshift, but after $\approx$30min increases exponentially
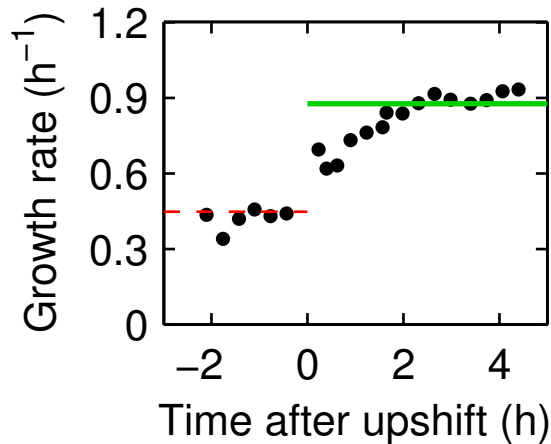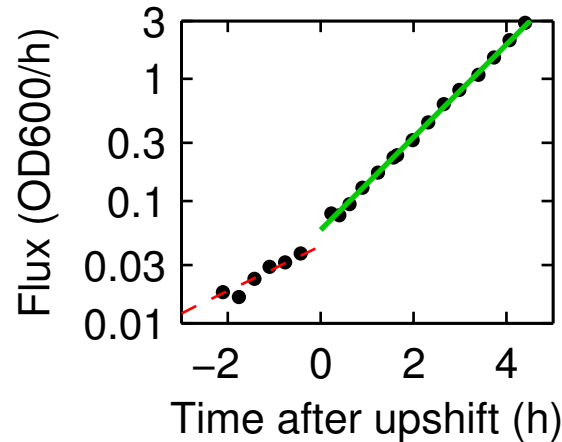
Figure 2.7: Long time flux for succinate add gluconate upshift. Wild-type NCM3722 cells were grown in minimal medium at 37°C with 1 mM IPTG and 0.4% succinate as the sole carbon source. At time zero gluconate was added to a final concentration of 20 mM. Culture saturation was avoided by serial dilution into a fresh, identical culture. The original culture was grown from -2.5h to 2h, the second culture from 1.3h to 3.3h, and the final culture from 3h to 4.7h. The raw OD600 data is reported in Table 7.4. Black points are flux calculated from two consecutive OD600 measurements. The data is stitched together to correct for dilution into sequential cultures. The red dashed line indicates the flux of the initial steady state culture conditions before upshift. The green solid line indicates the flux of the final steady state culture conditions after upshift.

with rate equal to the growth rate of the final steady state condition. In Chapter 3 we will base our model of carbon upshift on flux because of its relatively simple kinetics.

2.6   Resolving the growth rate - flux paradox

Growth rate and flux appear to have contradictory behavior. Flux has simple kinetics and quickly adjusts to its final behavior. However, growth rate does not quickly reach its final value and instead continues to increase slowly for several generations.

How can it be that the rate of mass increase (flux) is in its final state, but the exponential rate of mass increase (growth rate) does not reach its final state for several generations? In this section I resolve this apparent paradox by starting with a simple assumption. I will later derive the assumption from our model in Section 3.4.3.

Suppose that some time after carbon upshift protein mass increases as the sum

of a constant term and a term that grows exponentially with the final growth rate

$$M(t) = A + Be^{\lambda_f t} \tag{2.3}$$

for some constants A and B. Then flux as defined in Eq. (2.2) grows exponentially

$$J(t) = B\lambda_f e^{\lambda_f t}. \tag{2.4}$$

But growth rate as defined in Eq. (2.1) is slowly increasing in time with the form

$$\lambda(t) = \lambda_f \frac{1}{1 + (A/B)\,e^{-\lambda_f t}} \tag{2.5}$$

and only reaches λ_f after several generations. The simple assumption in Equation (2.3) produces the apparently contradictory observations of flux and growth rate shortly after carbon upshift.

That protein mass should take the form hypothesized in Equation (2.3) is not intuitive. We will derive the form from our model in Section 3.4.3, but will provide here a brief discussion about how such a form arises. The biomass consists of an exponentially growing term and a constant term. The exponentially growing term is expected because bacteria in a good environment grow exponentially. The constant term represents protein mass that is not growing. These proteins were produced in the initial growth condition, but are no longer produced in the final growth condition. These proteins are useless for growth in the new condition and are no longer being produced. Instead, these proteins are simply diluted away by cell growth.

2.7   Acknowledgments

Chapter 3

A simple analytical model of carbon upshift

3.1   Introduction

In this chapter we develop and solve our quantitative model of carbon upshift. The model is able to capture the fast increase of flux observed on the timescale of several minutes (see Figure 2.6) as well as the slow relaxation of growth rate over much longer timescales (see Figure 2.4) so that the entire growth curve is explained. The model is conceptually simple and analytically solvable. We do not attempt to capture the details of metabolic changes below the timescale of several minutes and are thus alleviated from explicitly considering the complex molecular details of underlying regulations. Instead, we only use the steady state growth observations (ribosome line and catabolic line) and the known topology of the regulatory interactions. At most there is only a single free parameter.

3.2   Model derivation

3.2.1   Qualitative description of the model

Figure 3.1 provides a cartoon summary of the structure of the model. Carbon enters metabolism at the left and eventually leaves as protein biomass at the right. Carbon
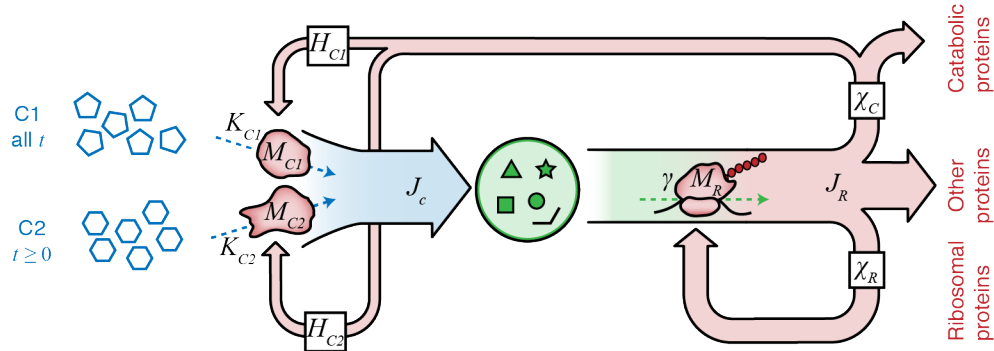
Figure 3.1: Cartoon summary of the carbon upshift model. We take a coarse-grained view of metabolism, focusing on the biosynthesis of protein (red) from the carbon influx (blue). Carbon enters the metabolism at the left by the activity of appropriate catabolic enzymes. The total carbon flux is composed of the flux of both carbon sources. Moving from left to right, the carbon is converted into various metabolites (*e.g.* carbon precursors, amino acids, charged tRNAs) depicted in green. The charged tRNAs are incorporated into proteins by the ribosomes. These proteins include ribosomal and catabolic proteins.

influx is catalyzed by the uptake systems specific to the two carbon sources present. The two uptake systems are regulated only by general catabolic control (via cAMP-CRP, which responds to the total carbon flux) and the sugar-specific auto-regulation. The carbon influx is balanced with outflux to protein by a time-dependent ribosome activity. The ribosomes are regulated in response to the availability of precursors (*e.g.* charged tRNA).

3.2.2 Quantitative formulation of the model

The rate of increase of protein mass M is, by definition, the total protein synthesis flux J_R

$$J_R \equiv \frac{dM}{dt}. \tag{3.1}$$

Protein synthesis is given by

$$\frac{d}{dt}M_R = \chi_R(t) \cdot J_R(t), \tag{3.2}$$

$$\frac{d}{dt}M_{C1} = H_{C1}(t) \cdot \chi_C(t) \cdot J_R(t), \tag{3.3}$$

$$\frac{d}{dt}M_{C2} = H_{C2}(t) \cdot \chi_C(t) \cdot J_R(t). \tag{3.4}$$

The catabolic proteins (M_{C1} and M_{C2}) are the rate-limiting enzymes for the catabolic influx of the carbon sources C1 and C2, respectively. All protein synthesis is a result of the action of ribosomes, composed of the ribosomal proteins (M_R). $\chi_R(t)$ and $\chi_C(t)$ are the fraction of total protein synthesis devoted to ribosomal proteins and catabolic enzymes, respectively, and summarize the regulation of these proteins. $H_{C1}(t)$ and $H_{C2}(t)$ are the sugar-specific regulatory functions (*e.g.* the transcriptional repression of the *lac* operon by LacI) and capture the fraction of catabolic protein synthesis devoted the enzymes M_{C1} and M_{C2}, respectively. Carbon source C1 is always present so $H_{C1}(t) = h_{C1}$ is constant for all time. To capture the expression of the rate-limiting enzyme responsible for the catabolism of carbon source C2, $H_{C2}(t)$ increases from an initial constant value to h_{C2} at the time zero (when C2 is added to the medium).

3.2.3 Ribosome regulatory function

Mechanistically, $\chi_R(t)$ is set by a number of factors, with a major one being the tRNA charging level (which modulates the synthesis of ppGpp) [32]. To keep the description contained within the essential dynamical variables introduced above, we note that the tRNA charging level is reflected in the translational activity, defined as

$$\gamma \equiv \frac{J_R}{M_R}. \tag{3.5}$$

We then make the Ansatz that $\chi_R(t)$ *depends on time only through* $\gamma(t)$, *i.e.*,

$$\chi_R(t) = f_R(\gamma(t)). \tag{3.6}$$

To find the form of the function $f_R(\gamma)$, our strategy is to use the steady state experimental knowledge of the ribosomal mass fraction, $\phi_R \equiv M_R/M$. First we define the instantaneous growth rate

$$\lambda(t) \equiv \frac{d}{dt} \ln(M) = \frac{1}{M} \frac{dM}{dt}. \tag{3.7}$$

Next, using Eqs. (3.1) and (3.2) and the definitions of ϕ_R and $\lambda(t)$, we write the

evolution equation for $\phi_R(t)$,

$$\frac{d}{dt}\phi_R = \lambda(t) \cdot [\chi_R(t) - \phi_R] \tag{3.8}$$

which gives in steady state

$$\phi_R^* = \chi_R^* = f_R(\gamma^*), \tag{3.9}$$

where we use asterisks to denote the steady-state values. Empirically, ϕ_R^* follows a linear relation with the steady-state growth rate, λ^*, as described above in Section 1.2.1,

$$\phi_R^* = \phi_{R,\min} + \lambda^*/\gamma_{\max} \tag{3.10}$$

Furthermore, from the definitions Eqs. (3.1), (3.5), and (3.6)

$$\lambda(t) = \frac{J_R}{M} = \gamma(t) \cdot \phi_R(t), \tag{3.11}$$

which in steady state is

$$\lambda^* = \gamma^* \cdot \phi_R^*. \tag{3.12}$$

Using Eq. (3.12) in Eq. (3.10) and solving for ϕ_R^*, we finally obtain

$$f_R(\gamma^*) = \phi_R^* = \frac{\phi_{R,\min}}{1 - \gamma^*/\gamma_{\max}}. \tag{3.13}$$

It will be useful to express the medium-independent constant $\phi_{R,min}$ in terms of other dynamical variables. In the final steady state growth condition with growth rate $\lambda^* = \lambda_f$ and translational activity $\gamma^* = \gamma_f$, we find from Eqs. (3.10) and (3.12)

$$\phi_{R,min} = \frac{\lambda_f}{\gamma_f}\left(1 - \frac{\gamma_f}{\gamma_{max}}\right) \tag{3.14}$$

and rewrite Eq. (3.13)

$$f_R(\gamma^*) = \phi_R^* = \frac{\lambda_f}{\gamma_f}\left(\frac{1 - \gamma_f/\gamma_{\max}}{1 - \gamma^*/\gamma_{\max}}\right). \tag{3.15}$$

3.2.4   Catabolic regulatory function

We now take the same strategy to determine $\chi_C(t)$. Mechanistically, $\chi_C(t)$ is set by carbon precursors, whose levels mirror the levels of amino acids and thus the level of tRNA charging, with the latter reflected in the translational activity γ. We make the ansatz that $\chi_C(t)$ *depends on time only through* $\gamma(t)$, *i.e.*,

$$\chi_C(t) = f_C(\gamma(t)). \tag{3.16}$$

Next, we write the evolution equation for the mass fraction of one of the catabolic enzymes $\phi_C \equiv M_{C1}/M$ using Eqs. (3.1) and (3.3) and the definition of $\lambda(t)$ from Eq. (3.7)

$$\frac{d}{dt}\phi_{C1} = \lambda(t) \cdot [h_{C1}(t)\chi_C(t) - \phi_{C1}], \tag{3.17}$$

which gives in steady state

$$\chi_C^* = f_C(\gamma^*) = \phi_{C1}^*/h_{C1}. \tag{3.18}$$

We consider catabolic enzymes that are activated by cAMP-Crp so that we know empirically that under carbon limited conditions ϕ_{C1}^* follows a linear relation with the steady-state growth rate

$$\phi_{C1}^* = h_{C1}(1 - \lambda^*/\lambda_C), \tag{3.19}$$

as described above in Section 1.2.3. Using the steady state growth rate from Eq. (3.12) and ϕ_R^* from Eq. (3.15) in Eq. (3.19),

$$f_C(\gamma^*) = \frac{\phi_{C1}^*}{h_{C1}} = 1 - \frac{\lambda_f}{\lambda_C}\frac{\gamma^*}{\gamma_f}\left(\frac{1 - \gamma_f/\gamma_{\max}}{1 - \gamma^*/\gamma_{\max}}\right). \tag{3.20}$$

Finally, we have the forms of $\chi_R(t)$ and $\chi_C(t)$,

$$\chi_R(t) = f_R(\gamma(t)) = \frac{\lambda_f}{\gamma_f}\left(\frac{1 - \gamma_f/\gamma_{\max}}{1 - \gamma(t)/\gamma_{\max}}\right), \tag{3.21}$$

$$\chi_C(t) = f_C(\gamma(t)) = 1 - \frac{\lambda_f}{\lambda_C}\frac{\gamma(t)}{\gamma_f}\left(\frac{1 - \gamma_f/\gamma_{\max}}{1 - \gamma(t)/\gamma_{\max}}\right) = 1 - \frac{\gamma(t)}{\lambda_C}\chi_R(t). \tag{3.22}$$

3.2.5 The central differential equation

Catabolic proteins determine the carbon flux

$$J_C(t) = K_{C1}(t)M_{C1} + K_{C2}(t)M_{C2}. \tag{3.23}$$

$K_{C1}(t)$ and $K_{C2}(t)$ are the catabolic rate functions, with $K_{C1}(t) = k_{C1}$ constant for all time, and $K_{C2}(t)$ jumping from 0 to constant k_{C2} at $t = 0$ with the addition of carbon source $C2$. When carbon source $C2$ becomes available at $t = 0$ the carbon influx J_C jumps instantaneously to a new value determined by the product of k_{C2} and the initial condition $M_{C2}(t = 0)$. Flux changes on a much faster timescale than protein mass, and thus we assume instantaneous flux balance to prevent the buildup of intermediate metabolites, *i.e.*,

$$J(t) \equiv J_R(t) = J_C(t), \tag{3.24}$$

where we have absorbed the constant carbon efficiency c_0, relating the carbon and protein flux, into the catabolic rate constants [28].

Equations (3.1) - (3.5) and (3.21) - (3.24) completely define the dynamics of the growth transition. These equations can be further simplified: using Eqs. (3.3), (3.4), (3.23), and (3.24), we get for $t > 0$

$$\frac{d}{dt}J = \frac{1}{T}\chi_C(t) \cdot J(t), \tag{3.25}$$

with

$$T \equiv \frac{1}{h_{C1}k_{C1} + h_{C2}k_{C2}}. \tag{3.26}$$

Expressing the above in terms of $\gamma(t)$ defined in Eq. (3.5) and using also Eq. (3.2), we get

$$\frac{d}{dt}\gamma = \gamma(t)\left[\frac{1}{T}\chi_C(t) - \gamma(t)\chi_R(t)\right], \tag{3.27}$$

a closed equation for $\gamma(t)$. From its solution, we can obtain $M_R(t)$ from Eq. (3.2), or equivalently,

$$\frac{d}{dt}\ln(M_R) = \chi_R(t) \cdot \gamma(t). \tag{3.28}$$

The flux $J_R(t)$ is finally obtained from $\gamma(t)$ and $M_R(t)$ via Eq. (3.5), and the growth

curve $M(t)$ is obtained from $J_R(t)$ via Eq. (3.1).

3.2.6 Translational activity at the instant of upshift

Solution of the model amounts to solving the differential equation for translational activity Eq. (3.27). The kinetics of translational activity are then used to solve for all of the other observables as already described.

All of the upshift observables can be expressed in terms of only steady state observables and the initial condition of the differential equation for translational activity. This initial condition is defined by γ_0, the translational activity at the instant of upshift. Translational activity, by definition (Eq. (3.5)), is the ratio of flux and ribosomal protein mass. In many cases the flux and ribosomal mass are the same in the instant of upshift as they were in the previous instant so that the translational activity at the instant of upshift is equal to the translational activity of the initial steady state growth condition $(\gamma_0 = \gamma_i)$.

If the added carbon source is immediately taken up by the cell the translational activity at the instant of upshift exceeds the translational activity of the initial steady state condition. Using the definition of γ in Eq. (3.5) and the flux balance assumption Eq. (3.24)

$$\gamma_0 = \gamma_i + \frac{\Delta J_{C,0}}{M_{R,0}}, \tag{3.29}$$

where $\Delta J_{C,0}$ is the additional carbon flux at the instant of upshift and $M_{R,0} \equiv M_R(t=0)$ is the mass of ribosomal protein at the moment of upshift. The value of $M_{R,0}$ is known from steady state measurements of ribosome abundance. Equivalently, since catabolic proteins determine carbon flux,

$$\gamma_0 = \gamma_i + \frac{k_{C2} M_{C2}(t=0)}{M_{R,0}}. \tag{3.30}$$

Thus the translational activity at the instant of upshift is determined by the carbon flux, or equivalently the abundance of the relevant catabolic proteins, at the instant of upshift. If the cell cannot immediately metabolize the new carbon source at the instant of upshift, $\gamma_0 = \gamma_i$ and the translational activity is continuous at the moment of upshift. However, if the cell immediately utilizes the added carbon source at the instant of upshift, $\gamma_0 > \gamma_i$

and the translational activity is discontinuous at $t = 0$.

3.3   Comparison to the Instantaneous Rates model

Now that the model has been completely defined, we compare our model to the model developed by Bremer and Dennis [31]. Their model makes quantitative predictions about the kinetics of protein synthesis throughout a nutritional upshift from minimal medium to broth (rich medium). The model assumes, based on observations, that the exponential rate of ribosome synthesis immediately changes from the initial steady state growth rate to the final steady state growth rate at the instant of upshift. Additionally, they take the translational activity to change instantaneously from the initial to the final steady state value at the instant of upshift. Using only these two features, the model is capable of making quantitative predictions of the kinetics of protein mass accumulation. Because of the instantaneous jump in the rates we refer to the model as the "Instantaneous Rates" (IR) model.

Comparison with our model reveals that the two models are identical if the rate γ (the translational activity) instantaneously jumps from initial to the final steady state value at the instant of upshift. In our model the rates are instead determined by the relative values of the nutrient influx and protein outflux. Although the models are identical in this particular situation, in general the models give quantitatively different predictions. However, it is also worth mentioning here that our model is approximately equivalent to the IR model if the final steady state growth rate is close to the intercept of the catabolic line ($\lambda_f \approx \lambda_C$). This is because, as will be discussed in Section 3.4.1, the kinetics of the translational activity γ are very fast when the final growth rate is close to the intercept of the catabolic line so that the change in the rates is nearly instantaneous. Throughout this chapter we will check that our results match the predictions of the IR model in these two regimes.

Our model offers several advantages over the IR model. The IR model implicitly assumes the the cells know about the final growth state at the instant of upshift. In our model the regulatory functions guide the cell to its final steady state using only knowledge of the present. The IR model does not explicitly consider catabolic (or other

metabolic) proteins; our model provides quantitative predictions of the expression of catabolic proteins.

There are two situations in which our model is identical to the IR model and in both cases there is an explanation of why the rates quickly jump to their final values. The first case is when the translational activity instantly jumps to the final steady state value at the instant of upshift. In our model this only happens when the cell already has the proteins responsible for the metabolism of the added nutrient (see Eq. (3.30)). The other case is when the final steady state growth rate is close to the intercept of the catabolic line. Being near the intercept of the catabolic line means that there is very little expression of catabolic genes. Thus the cell does not need to make many catabolic proteins to produce the requisite carbon flux. The cell makes the catabolic proteins very quickly so all of the rates quickly relax to the final steady state values.

3.4   Model solution

3.4.1   Kinetics of translational activity

We now solve for the kinetics of translational activity. Substituting Eqs. (3.21) and (3.22) in Eq. (3.27) we solve for the steady state and discover

$$T = \frac{1}{\lambda_f}\left(1 - \frac{\lambda_f}{\lambda_C}\right).$$ (3.31)

We rearrange Eq. (3.27) using Eqs. (3.21), (3.22) and (3.31) to find the form

$$\frac{d\gamma}{dt} = \frac{1}{T}f(\gamma)$$ (3.32)

with the forcing function $f(\gamma)$

$$f(\gamma) \equiv \gamma\left(\frac{1 - \gamma/\gamma_f}{1 - \gamma/\gamma_{\max}}\right).$$ (3.33)

Figure 3.2 shows the forcing function for an upshift with final growth rate $1.0\,\mathrm{h}^{-1}$. The corresponding potential function $U(\gamma) \equiv -\int^{\gamma} f(\gamma')d\gamma'$ is also plotted. The translational activity γ has only one stable fixed point in the domain $0 \leq \gamma \leq \gamma_{\max}$. The stable

(a)   **(b)**
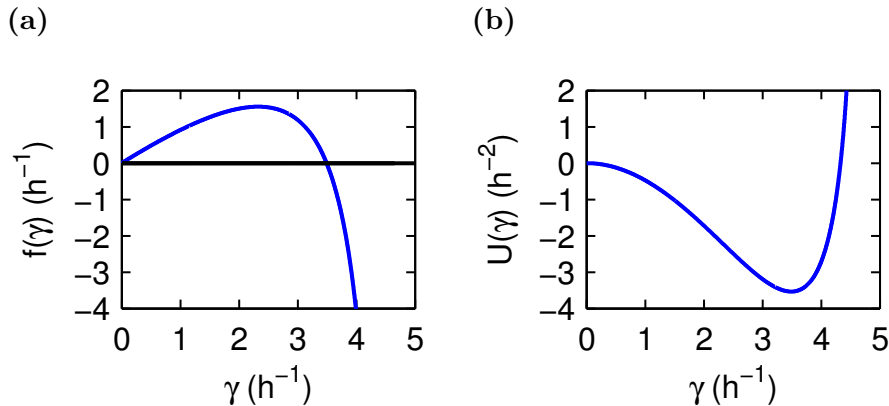
Figure 3.2: Translational activity forcing function and corresponding potential function. The solution of the forcing function $f(\gamma)$ (a) and the corresponding potential function $U(\gamma)$ (b) for an upshift with final growth rate $1.0\,\mathrm{h}^{-1}$.

fixed point is the final translational activity γ_f. Since Eq. (3.32) is first-order and has only one stable fixed point, the solution always monotonically approaches that point (*i.e.* no overshooting and no oscillations) [33]. Thus, throughout carbon upshift, the translational activity always monotonically approaches the final translational activity.

We rearrange Eq. (3.32) using Eq. (3.33)

$$dt = d\gamma \frac{T}{\gamma(t)} \left(\frac{1 - \gamma(t)/\gamma_{\mathrm{max}}}{1 - \gamma(t)/\gamma_f} \right) \tag{3.34}$$

and integrate to find

$$t = T \ln \left[\left(\frac{\gamma(t)}{\gamma_0} \right) \left(\frac{1 - \gamma_0/\gamma_f}{1 - \gamma(t)/\gamma_f} \right)^{1 - \gamma_f/\gamma_{\mathrm{max}}} \right]. \tag{3.35}$$

Figure 3.3 demonstrates the kinetics of $\gamma(t)$ for an upshift with initial growth rate $0.4\,\mathrm{h}^{-1}$ and final growth rate $1.0\,\mathrm{h}^{-1}$ and $\gamma_0 = 2.8\,\mathrm{h}^{-1}$. Before upshift, the culture is in steady state exponential growth and γ is constant. The upshift occurs at $t = 0$ and there is an immediate jump to γ_0. The translational activity then relaxes to γ_f as described by Eq. (3.35). The translational activity approaches the final value asymptotically and almost all of the change occurs for $t < 0.2\mathrm{h} = 12\mathrm{min}$, a short timescale compared to bacterial growth.

To determine the explicit time dependence just after upshift, we Taylor expand
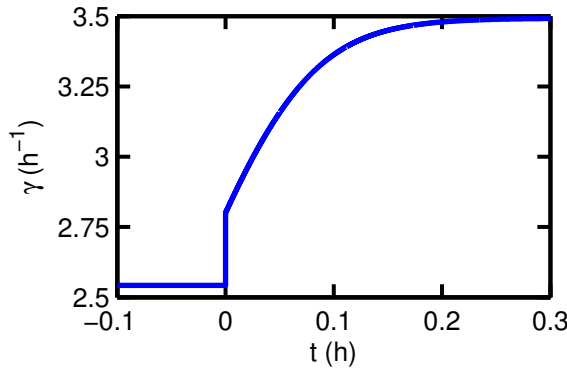
Figure 3.3: Exact solution of translational activity throughout upshift. The solution of translational activity $\gamma(t)$ for an upshift with initial growth rate $0.4\,\mathrm{h}^{-1}$ and final growth rate $1.0\,\mathrm{h}^{-1}$ and $\gamma_0 = 2.8\,\mathrm{h}^{-1}$.

Eq. (3.35) about $\gamma \approx \gamma_0$ and $t \approx 0$ and find that the translational activity is linear in time

$$\gamma(t \approx 0) \approx \gamma_0 + \gamma_0' t \tag{3.36}$$

with slope

$$\gamma_0' \equiv \frac{\gamma_0}{T}\left(\frac{1 - \gamma_0/\gamma_f}{1 - \gamma_0/\gamma_{\max}}\right). \tag{3.37}$$

The translational activity instantly heads in the direction of the final value; $\gamma_0' > 0$ for $\gamma_0 < \gamma_f$ and vice versa.

To examine the long time behavior of the translational activity, we Taylor expand Eq. (3.35) about $\gamma(t \gg 0) \approx \gamma_f$ and find that the translational activity exponentially approaches the final value

$$\gamma(t \gg 0) = \gamma_f - (\gamma_f - \gamma_0)\left(\frac{\gamma_f}{\gamma_0}\right)^{\frac{1}{1 - \gamma_f/\gamma_{\max}}} e^{-\frac{t}{T(1 - \gamma_f/\gamma_{\max})}}. \tag{3.38}$$

In the IR model the translational activity is assumed to jump instantaneously from its initial value to its final steady state value at the moment of upshift. Obviously then the models are identical for $\gamma_0 = \gamma_f$. Note that the timescale of relaxation of translational activity in both regimes scales with T according to Eqs. (3.36)-(3.38). From Eq. (3.31) $T \approx 0$ when $\lambda_f \approx \lambda_C$. Thus when the final steady state growth rate approached the intercept of the catabolic line, the timescale of translational activity relaxation approaches zero. For fast enough final growth rate, the relaxation of transla-

tional activity is essentially instantaneous and our model gives the same result as the IR model.

3.4.2 Kinetics of protein synthesis flux

Before upshift, the cells are in steady state exponential growth and protein synthesis flux (or flux, for short) grows exponentially with the initial growth rate λ_i

$$J(t < 0) = J_{i,0}e^{\lambda_i t}, \tag{3.39}$$

or equivalently

$$\ln\left(J(t < 0)\right) = \lambda_i t + ln\left(J_{i,0}\right), \tag{3.40}$$

with flux just before upshift

$$J_{i,0} \equiv M_{R,0}\gamma_i. \tag{3.41}$$

At the moment of upshift, translational activity jumps to the initial condition value γ_0 and according to Eq. (3.5) flux instantly jumps to its new value

$$J(t = 0) = M_{R,0}\gamma_0 = J_{i,0}\frac{\gamma_0}{\gamma_i}. \tag{3.42}$$

To determine the kinetics of flux after upshift, we integrate Eq. (3.28) directly using Eq. (3.34) to substitute for dt to find

$$M_R(\gamma) = M_{R,0}\left(\frac{1 - \gamma_0/\gamma_f}{1 - \gamma(t)/\gamma_f}\right)^{(1-\lambda_f/\lambda_C)(1-\gamma_f/\gamma_{\max})} \tag{3.43}$$

and

$$J_R(\gamma) = M_{R,0}\gamma(t)\left(\frac{1 - \gamma_0/\gamma_f}{1 - \gamma(t)/\gamma_f}\right)^{(1-\lambda_f/\lambda_C)(1-\gamma_f/\gamma_{\max})}. \tag{3.44}$$

We simplify the expression for J by using Eq. (3.35) in Eq. (3.44)

$$J_R(t) = J_{i,0}\left(\frac{\gamma_0}{\gamma_i}\right)\left(\frac{\gamma(t)}{\gamma_0}\right)^{\lambda_f/\lambda_C}e^{\lambda_f t}, \tag{3.45}$$
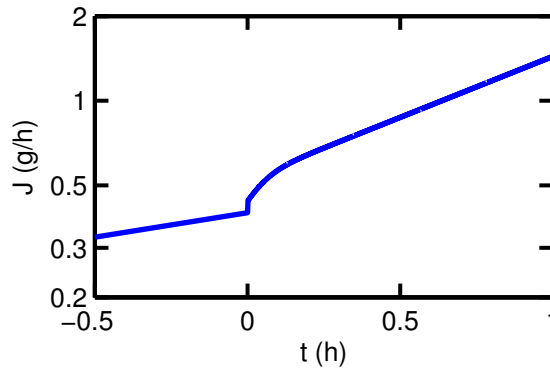
Figure 3.4: Exact solution of flux throughout upshift. The solution of $J(t)$ from the model for an upshift with initial growth rate $0.4\,h^{-1}$ and final growth rate $1.0\,h^{-1}$ and $\gamma_0 = 2.8\,h^{-1}$. Soon after upshift, flux J grows exponentially with rate equal to the final growth rate.

or equivalently,

$$\ln\left[J(t)\right] = \lambda_f t + \frac{\lambda_f}{\lambda_C} \ln\left[\frac{\gamma(t)}{\gamma_0}\right] + \ln\left[J_{i,0}\frac{\gamma_0}{\gamma_i}\right]. \tag{3.46}$$

Figure 3.4 demonstrates the kinetics of $J(t)$ for an upshift with initial growth rate $0.4\,h^{-1}$ and final growth rate $1.0\,h^{-1}$ and $\gamma_0 = 2.8\,h^{-1}$ (the same upshift as Figure 3.3 for $\gamma(t)$). Before upshift, the culture is in steady state exponential growth and J grows with the initial growth rate. The upshift occurs at $t = 0$ and there is an immediate jump due to the discontinuity in γ. Flux grows with final growth rate after γ has stopped changing significantly (for $t > 0.2h = 12$min as above), but initially grows more quickly.

To understand the behavior of flux just after upshift, we use Eq. (3.36) in Eq. (3.46) and Taylor expand near $t \approx 0$ to find that flux increases exponentially

$$\ln\left[J(t \approx 0)\right] \approx \lambda_f \left(1 + \frac{\gamma'_0}{\gamma_0 \lambda_C}\right) t + \ln\left[J_{i,0}\frac{\gamma_0}{\gamma_i}\right]. \tag{3.47}$$

Typically $\gamma_0 < \gamma_f$ so that γ is increasing ($\gamma'_0 > 0$) and, from Eq. (3.47), flux initially increases faster than λ_f. However, if $\gamma_0 > \gamma_f$, γ is decreasing and flux initially increases slower than γ_f.

Sufficiently long after upshift, $\gamma(t \gg 0) \approx \gamma_f$ and, from Eq. (3.46), the flux grows with rate λ_f

$$\ln\left[J(t \gg 0)\right] \approx \lambda_f t + \ln\left[J_{i,0}\right] + \ln\left[D\right] \tag{3.48}$$

with constant asymptotic flux discontinuity

$$D \equiv \frac{\gamma_0}{\gamma_i} \left(\frac{\gamma_f}{\gamma_0} \right)^{\frac{\lambda_f}{\lambda_C}}. \tag{3.49}$$

If flux is observed at a coarse level only the asymptotic behaviors are apparent and Eqs. (3.40) and (3.48) describe its kinetics. Then the flux has an apparent discontinuity at $t = 0$. The asymptotic flux discontinuity D measures the apparent discontinuity. D is not a real discontinuity because the short time kinetics deviate from this long time approximation. However, D is an easily observable number that summarizes the upshift and is influenced by the short time kinetics.

Bremer and Dennis IR Model predicts an analogous flux discontinuity

$$D_{IR} = \frac{\gamma_f}{\gamma_i}. \tag{3.50}$$

If $\gamma_0 = \gamma_f$, the our model is mathematically equivalent to the IR Model and $D(\gamma_0 = \gamma_f) = D_{IR}$. For fast final growth rate we also observe $D(\lambda_f \approx \lambda_C) \approx D_{IR}$, as expected.

3.4.3 Kinetics of protein mass

Before upshift, total protein mass grows exponentially with the initial growth rate $M(t < 0) = M_0 e^{\lambda_i t}$, where $M_0 \equiv M(t = 0)$ is the protein mass at the moment of upshift. We note that the mass of ribosomes and total protein at the instant of upshift are known from steady state measurements $M_{R,0}/M_0 = \phi_R^*(\lambda^* = \lambda_i)$.

To determine the behavior of the growth curve $M(t)$ after the upshift, we use $J(t)$ from Eq. (3.44) and dt from Eq. (3.34) to integrate Eq. (3.1) directly. The result is simplified using T from Eq. (3.31)

$$M(\gamma(t)) = M_0 \left(1 - \frac{\lambda_i \gamma_f}{\lambda_f \gamma_i} \left(\frac{1 + T\lambda_C \gamma_0/\gamma_{\max}}{1 + T\lambda_C \gamma_f/\gamma_{\max}} \right) \right) \tag{3.51}$$

$$+ M_0 \frac{\lambda_i \gamma_f}{\lambda_f \gamma_i} \left(\frac{1 + T\lambda_C \gamma(t)/\gamma_{\max}}{1 + T\lambda_C \gamma_f/\gamma_{\max}} \right) \left(\frac{\gamma_f - \gamma_0}{\gamma_f - \gamma(t)} \right)^{\left(1 - \frac{\lambda_f}{\lambda_C}\right)\left(1 - \frac{\gamma_f}{\gamma_{\max}}\right)}.$$

Note that the first term is constant and all of the time dependence manifests itself in the second term.
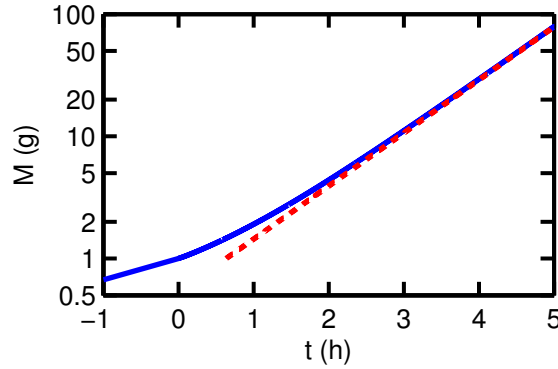
Figure 3.5: Exact solution of protein mass throughout upshift. The solution of protein mass $M(t)$ from the model for an upshift with initial growth rate $0.4\,\mathrm{h}^{-1}$ and final growth rate $1.0\,\mathrm{h}^{-1}$ and $\gamma_0 = 2.8\,\mathrm{h}^{-1}$. The exact solution of the model is the solid blue curve. The dashed red curve is an extrapolation of the final steady state behavior.

We rewrite M using Eq. (3.35)

$$
\begin{aligned}
M(t) =& M_0 \left(1 - \frac{\lambda_i \gamma_f}{\lambda_f \gamma_i} \left(\frac{1 + T\lambda_C \gamma_0 / \gamma_{\max}}{1 + T\lambda_C \gamma_f / \gamma_{\max}} \right) \right) \\
&+ M_0 \frac{\lambda_i \gamma_f}{\lambda_f \gamma_i} \left(\frac{1 + T\lambda_C \gamma(t)/\gamma_{\max}}{1 + T\lambda_C \gamma_f / \gamma_{\max}} \right) \left(\frac{\gamma_0}{\gamma(t)} \right)^{(1 - \lambda_f / \lambda_C)} e^{\lambda_f t},
\end{aligned}
\tag{3.52}
$$

and again $M(t)$ is the sum of a constant and another term containing all of the time dependence.

Figure 3.5 demonstrates the kinetics of $M(t)$ (blue) for an upshift with initial growth rate $0.4\,\mathrm{h}^{-1}$ and final growth rate $1.0\,\mathrm{h}^{-1}$ and $\gamma_0 = 2.8\,\mathrm{h}^{-1}$ (the same upshift as in the figures above). Before upshift, the culture is in steady state exponential growth and M grows with the initial growth rate. The upshift occurs at $t = 0$ and protein mass gradually increases its rate of growth. An extrapolation of the long time behavior of M with exponential rate equal to the final growth rate is shown as a red dashed curve. Comparing to the behavior of protein mass, it is clear that the culture is not growing with the final growth rate even as long as 2h after upshift.

3.4.4 Protein mass kinetics are related to the proteome composition

The above equations do not provide much insight into the meaning of the large constants in $M(t)$, but we know that at sufficiently long times the behavior of $M(t)$

should be simple. We combine Eqs. (3.1) and (3.5)

$$dM = \gamma M_R dt \tag{3.53}$$

and integrate from $t = 0$ to $t = \tau$

$$M(t = \tau) - M_0 = \int_{t'=0}^{\tau} \gamma(t') M_R(t') dt'. \tag{3.54}$$

We choose τ such that $\gamma(t \geqslant \tau) \approx \gamma_f$ (*i.e.* γ is no longer changing significantly). Then

$$M(t > \tau) - M_0 \approx \int_{t'=0}^{\tau} \gamma(t') M_R(t') dt' + \gamma_f \int_{t'=\tau}^{t} M_R(t') dt'. \tag{3.55}$$

We can integrate the second term by first calculating M_R from Eq. (3.28) using the steady state relationships in Eqs. (3.9) and (3.12) to simplify the result

$$M_R(t \geqslant \tau) = M_R(t = \tau) e^{\lambda_f(t-\tau)}. \tag{3.56}$$

We substitute Eqs. (3.54) and (3.56) in Eq. (3.55) and find

$$M(t > \tau) \approx M(t = \tau)\left(1 - \frac{\phi_R(t = \tau)}{\phi_{R,f}}\right) + M(t = \tau)\frac{\phi_R(t = \tau)}{\phi_{R,f}} e^{\lambda_f(t-\tau)}, \tag{3.57}$$

where the constant $\phi_{R,f}$ is the ribosomal mass fraction in the final steady state growth condition. At sufficiently long times protein has the expected exponentially growing term, but also has a constant term! Protein mass accumulates by the activity of ribosomes so it makes sense that protein grows exponentially and proportional to the mass fraction of ribosomes. The non-growing term is proportional to the deficit of ribosomal mass fraction relative to the final ribosomal mass fraction, *i.e.* the mass fraction that will be ribosomal in the final steady state but is not ribosomal yet. This mass fraction is made up of proteins that had higher expression in the past than they have in the final steady state. Thus the constant term is the result of proteins that are left over from the culture's history but are unwanted in the final state. These proteins are diluted away by exponential growth so that they are negligible in the final steady state.

It is possible for the transient ribosome expression to be large enough that the

ribosomal mass fraction transiently exceeds the final steady state value. In this case the non-growing term is negative. The surplus of ribosome mass fraction comes with the cost; there is a deficit of the mass fraction of some other proteins. Thus a constant negative term is the result of proteins that were not expressed highly enough in the past, but are wanted in the final steady state.

3.4.5 Upshift kinetics are approximated by an effective lag time

This analysis provides insight about the meaning of the terms describing protein at long times, but does not provide the quantitative behavior because of the presence of $M(t = \tau)$. To provide a quantitative form we use Eq. (3.52) sufficiently long after upshift when $\gamma(t \gg 0) \approx \gamma_f$ is constant to find

$$M(t \gg 0) = M_0 \left(1 - \frac{\lambda_i \gamma_f}{\lambda_f \gamma_i} \left(\frac{1 + T\lambda_C \frac{\gamma_0}{\gamma_{\max}}}{1 + T\lambda_C \frac{\gamma_f}{\gamma_{\max}}} \right) \right) + M_0 \frac{\lambda_i \gamma_f}{\lambda_f \gamma_i} \left(\frac{\gamma_0}{\gamma_f} \right)^{(1 - \frac{\lambda_f}{\lambda_C})} e^{\lambda_f t}, \quad (3.58)$$

which is of the same form as Eq. (3.57), *i.e.* the sum of a constant term and a term that grows exponentially with rate λ_f. At even longer times the constant term is negligible and

$$M(t \ggg 0) = M_0 \frac{\lambda_i \gamma_0}{\lambda_f \gamma_i} \left(\frac{\gamma_f}{\gamma_0} \right)^{\lambda_f / \lambda_C} e^{\lambda_f t}, \quad (3.59)$$

or equivalently,

$$M(t \ggg 0) = M_0 D \frac{\lambda_i}{\lambda_f} e^{\lambda_f t}. \quad (3.60)$$

This behavior is plotted in red in the figure for $M(t)$ above.

Sufficiently long after upshift, $M(t)$ grows exponentially with final growth rate as in Eq. (3.59). We define the lag time t_{lag} such that we can rewrite this exponential in the form

$$M(t \ggg 0) = M_0 e^{\lambda_f (t - t_{lag})}. \quad (3.61)$$

For the upshift in the figure above, the lag time is approximately $0.5h$. This is visible as the offset between the behavior of M (blue solid curve) and the extrapolation of the long time behavior (red dashed curve) in Figure 3.5. Like the asymptotic flux discontinuity D, the lag time t_{lag} provides a metric that summarizes the upshift. We find using Eqs. (3.59)

and (3.61)

$$t_{lag} = \frac{1}{\lambda_f} \ln \left[\frac{\lambda_f}{\lambda_i} \frac{\gamma_i}{\gamma_0} \left(\frac{\gamma_0}{\gamma_f} \right)^{\lambda_f/\lambda_C} \right],$$ (3.62)

or equivalently using the definition of D in Eq. (3.49),

$$t_{lag} = \frac{1}{\lambda_f} \ln \left[\frac{\lambda_f}{\lambda_i} \frac{1}{D} \right].$$ (3.63)

We compare to the lag time predicted by the IR Model

$$t_{lag,IR} = \frac{1}{\lambda_f} \ln \left[\frac{\lambda_f}{\lambda_i} \frac{\gamma_i}{\gamma_f} \right] = \frac{1}{\lambda_f} \ln \left[\frac{\lambda_f}{\lambda_i} \frac{1}{D_{IR}} \right].$$ (3.64)

If $\gamma_0 = \gamma_f$, our model is mathematically equivalent to the IR Model and $t_{lag} = t_{lag,IR}$. For fast final growth rate $\lambda_f \approx \lambda_C$, the lag time of the two models is approximately the same $t_{lag} \approx t_{lag,IR}$.

3.4.6   Kinetics of growth rate

We calculate the exact form of the growth rate λ using its definition Eq. (3.7) and Eqs. (3.44) and (3.51)

$$\lambda\left(\gamma(t)\right) = \lambda_f \frac{\left(\frac{\gamma(t)}{\gamma_f}\right) \left(\frac{1-\gamma_0/\gamma_f}{1-\gamma(t)/\gamma_f}\right)^{(1-\lambda_f/\lambda_C)(1-\gamma_f/\gamma_{\max})}}{\left(\frac{\gamma_i \lambda_f}{\gamma_f \lambda_i}\right) - \left(\frac{1+T\lambda_C\gamma_0/\gamma_{\max}}{1+T\lambda_C\gamma_f/\gamma_{\max}}\right) + \left(\frac{1+T\lambda_C\gamma(t)/\gamma_{\max}}{1+T\lambda_C\gamma_f/\gamma_{\max}}\right) \left(\frac{1-\gamma_0/\gamma_f}{1-\gamma(t)/\gamma_f}\right)^{\left(1-\frac{\lambda_f}{\lambda_C}\right)\left(1-\frac{\gamma_f}{\gamma_{\max}}\right)}}.$$ (3.65)

Figure 3.6 demonstrates the kinetics of growth rate λ for an upshift with initial growth rate $0.4\,\text{h}^{-1}$ and final growth rate $1.0\,\text{h}^{-1}$ and $\gamma_0 = 2.8\,\text{h}^{-1}$. Before upshift, the culture is in steady state exponential growth and growth rate is constant at $\lambda_i = 0.4\,\text{h}^{-1}$. The upshift occurs at time zero and, because of the immediate jump in translational activity, growth rate immediately jumps to $\lambda = \lambda_i \gamma_0/\gamma_i$. The growth rate then relaxes to λ_f as described by Eq. (3.65). The growth rate approaches the final steady state growth rate asymptotically over the course of several hours.

At long enough times that the translational activity has settled to its final value, we calculate the exact form for the instantaneous growth rate λ using the definition of

Figure 3.6: Exact solution of growth rate throughout upshift. The solution of $\lambda(t)$ from the model for an upshift with initial growth rate $0.4\,\mathrm{h}^{-1}$ and final growth rate $1.0\,\mathrm{h}^{-1}$ and $\gamma_0 = 2.8\,\mathrm{h}^{-1}$.

growth rate Eq. (3.7) and the exact form of $M(t \gg 0)$ in Eq. (3.58)

$$\lambda(t \gg 0) = \frac{\lambda_f}{1 + \left(\frac{\gamma_f}{\gamma_0}\right)^{\left(1 - \frac{\lambda_f}{\lambda_C}\right)} \left(\frac{\lambda_f \gamma_i}{\lambda_i \gamma_f} - \left(\frac{1 + T\lambda_C \frac{\gamma_0}{\gamma_{\max}}}{1 + T\lambda_C \frac{\gamma_f}{\gamma_{\max}}}\right)\right) e^{-\lambda_f t}}. \tag{3.66}$$

We also calculate a more simple and intuitive form like we did above for $M(t)$. From Eq. (3.57), $M(t)$ has a simple form at long enough times and combining with Eq. (3.7),

$$\lambda(t > \tau) \approx \lambda_f \frac{1}{1 + [\phi_{R,f}/\phi_R(t = \tau) - 1]\, e^{-\lambda_f(t-\tau)}}. \tag{3.67}$$

Instantaneous growth rate has a long timescale relaxation with rate λ_f. Typically, instantaneous growth rate asymptotically approaches λ_f from below. However, if ribosomal production overshoots enough the ribosomal mass fraction transiently exceeds the final value and instantaneous growth rate overshoots the final value (*i.e.* $\lambda > \lambda_f$)!

3.4.7 Kinetics of ribosomal proteins

Before upshift the culture is in steady state exponential growth and ribosomal proteins grow exponentially with the initial steady state growth rate

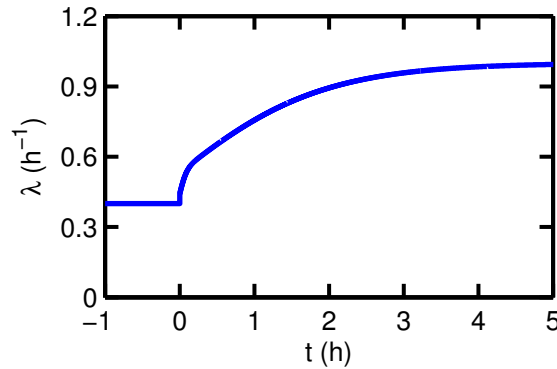$$M_R(t < 0) = M_{R,0} e^{\lambda_i t}. \tag{3.68}$$

Figure 3.7: Exact solution of ribosomal protein mass throughout upshift. The solution of $M_R(t)$ from the model for an upshift with initial growth rate $0.4\,\mathrm{h}^{-1}$ and final growth rate $1.0\,\mathrm{h}^{-1}$ and $\gamma_0 = 2.8\,\mathrm{h}^{-1}$.

The kinetics of ribosomal protein mass after upshift was already calculated as a function of the translational activity in Eq. (3.43). We simplify the expression using Eq. (3.35)

$$M_R(t) = M_{R,0}\left(\frac{\gamma_0}{\gamma(t)}\right)^{1-\lambda_f/\lambda_C} e^{\lambda_f t}. \tag{3.69}$$

Figure 3.7 demonstrates the kinetics of ribosomal protein mass $M_R(t)$ for an upshift with initial growth rate $0.4\,\mathrm{h}^{-1}$ and final growth rate $1.0\,\mathrm{h}^{-1}$ and $\gamma_0 = 2.8\,\mathrm{h}^{-1}$ (the same upshift that we have been discussing in the other sections). Before upshift, the culture is in steady state exponential growth and the ribosomal protein mass grows with the initial growth rate. The upshift occurs at $t = 0$ and over a short time the production rate of ribosomes changes. Quickly after upshift the production rate of ribosomal proteins reaches its final value and ribosomal protein mass grows exponentially with rate equal to the final steady state growth rate.

Sufficiently long after upshift the translational activity has reached its final steady state value ($\gamma(t \gg 0) \approx \gamma_f$) and

$$M_R(t \gg 0) = M_{R,0}\left(\frac{\gamma_0}{\gamma_f}\right)^{1-\lambda_f/\lambda_C} e^{\lambda_f t}. \tag{3.70}$$

If ribosomes are observed at a coarse level only the asymptotic behaviors are apparent and Eqs. (3.68) and (3.70) describe the kinetics. It has long been observed for other types of nutrient upshifts that the stable RNA, which is a proxy for ribosome abundance,

abruptly becomes exponential with rate equal to the final growth rate [34] [31].

3.4.8 Kinetics of catabolic proteins

Before upshift the culture is in steady state exponential growth and the catabolic proteins accumulate exponentially with the initial growth rate

$$M_{C1}(t < 0) = M_{C1,0}e^{\lambda_i t}, \tag{3.71}$$

where $M_{C1,0}$ is the mass of catabolic protein M_{C1} at time zero.

To determine the kinetics of the catabolic protein M_{C1} after upshift we integrate Eq. (3.3) directly using Eq. (3.22) to substitute for χ_C, Eq. (3.44) to substitute for J, and Eq. (3.34) to substitute for dt

$$M_{C1}(\gamma) = M_{C1,0} - h_1 J_{i,0} T \frac{\gamma_0}{\gamma_i} + h_1 J_{i,0} T \left(\frac{\gamma(t)}{\gamma_i} \right) \left(\frac{1 - \gamma_0/\gamma_f}{1 - \gamma(t)/\gamma_f} \right)^{\left(1 - \gamma_f/\gamma_{\max} \right)\left(1 - \lambda_f/\lambda_C \right)}. \tag{3.72}$$

We simplify the expression using Eq. (3.44)

$$M_{C1}(t) = M_{C1,0} + h_1 T \left(J(t) - \frac{\gamma_0}{\gamma_i} J_{i,0} \right). \tag{3.73}$$

The equations describing the accumulation of M_{C1} and M_{C2} are identical so

$$M_{C2}(t) = M_{C2,0} + h_2 T \left(J(t) - \frac{\gamma_0}{\gamma_i} J_{i,0} \right). \tag{3.74}$$

Figure 3.8 demonstrates the kinetics of catabolic protein mass $M_{C1}(t)$ for an upshift with initial growth rate $0.4\,\mathrm{h}^{-1}$ and final growth rate $1.0\,\mathrm{h}^{-1}$ and $\gamma_0 = 2.8\,\mathrm{h}^{-1}$ (the same upshift that we have been discussing in the other sections). Here we have chosen $h_{C1}=1$ for all time. Before upshift, the culture is in steady state exponential growth and the catabolic protein mass grows with the initial growth rate. The upshift occurs at $t = 0$ and over a short time the production rate of catabolic proteins changes. Quickly after upshift the production rate of catabolic proteins reaches its final value. Because the production rate of catabolic proteins decreases throughout carbon upshift, the amount of M_{C1} does not grow exponentially immediately, even though its production rate is
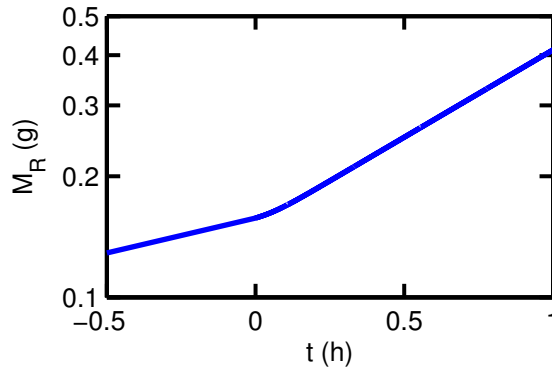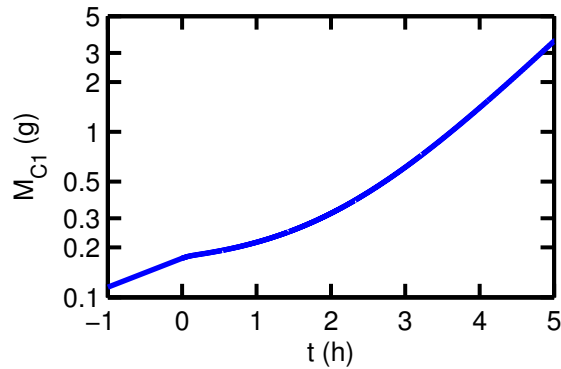
Figure 3.8: Exact solution of catabolic protein mass throughout upshift. The solution of $M_{C1}(t)$ from the model for an upshift with initial growth rate $0.4\,\mathrm{h}^{-1}$ and final growth rate $1.0\,\mathrm{h}^{-1}$ and $\gamma_0 = 2.8\,\mathrm{h}^{-1}$. Here we have chosen $h_{C1}=1$ for all time.

constant. The catabolic protein amount M_{C1} eventually grows exponentially with rate equal to the final steady state growth rate, but only after a period of apparent transient repression.

Bremer and Dennis' IR model does not consider the expression of catabolic proteins. The IR model assumes that the production rate of ribosomes and the translational activity instantly jump to their new values at the instant of upshift without explicitly considering the expression of the proteins needed to provide flux to the ribosomes. An important contribution of our model is that it also explicitly considers the expression of upstream metabolic proteins.

3.4.9 Solution for very high initial carbon flux

Note that in the above calculations no limit is placed on the translational activity and if the carbon flux is too high at the instant of upshift, the translational activity can transiently increase to unbounded levels. In reality something other than carbon (*e.g.* nitrogen) that has not been explicitly considered in the model, would become limiting so that the translational activity reaches a maximum value. In this section we develop an *ad hoc* method to deal with this problem within the existing model. Our method is to limit the translational activity so that it does not exceed a maximal value. We note that the considerations developed in this section are only needed in extreme conditions and only apply to one upshift of wild-type cells in this document. A proper understanding

of the behavior in such extreme conditions is outside the scope of this work and stands out as a possible future direction.

In steady state growth if carbon flux is not growth limiting, the growth rate is λ_C [14] and the translational activity, using Eq. (3.12), is

$$\gamma_C \equiv \frac{\lambda_C}{\phi_R{}^*\left(\lambda = \lambda_C\right)}. \tag{3.75}$$

We take γ_C to be the maximum translational activity during carbon upshift.

The existence of a maximum translational activity means that the protein synthesis flux $J = \gamma M_R$ also has a maximum and the cell cannot process all of the flux that the catabolic enzymes are capable of producing, defined as $J_{C,0}$. We hypothesize that flux is balanced as before and excess carbon flux leaks out of the cell, or carbon influx decreases so that it does not exceed ribosomal flux. Mechanistically, carbon flux could be limited by inducer exclusion whereby intermediate metabolites accumulate and inhibit the activity of the upstream catabolic enzymes so that flux is balanced with all ribosomes working with maximum activity [35]. Within the model this could be implemented by dynamically setting the values of $K_{C1}(t)$ and $K_{C2}(t)$ in Eq. (3.23) to keep flux balanced.

During this initial phase after upshift, the ribosomes work with activity that is constant in time $\gamma = \gamma_C$ and the regulation functions, from Eqs. (3.21) and (3.22), are also constant

$$\chi_R\left(\gamma = \gamma_C\right) = \lambda_C/\gamma_C, \tag{3.76}$$

$$\chi_C\left(\gamma = \gamma_C\right) = 0. \tag{3.77}$$

From Eqs. (3.77), (3.3) and (3.4), the catabolic enzymes do not increase during this time and thus the maximal carbon flux $J_{C,0}$ does not increase. Flux increases via ribosome accumulation until time τ_C when the ribosome amount has increased enough to process the maximal carbon flux with all ribosomes working at maximum translational activity

$$M_R(t = \tau_C) = J_{C,0}/\gamma_C. \tag{3.78}$$

From Eqs. (3.2) and (3.76), ribosome mass grows exponentially at maximal rate while

the translational activity is maximal

$$M_R(t \leqslant \tau_C) = M_{R,0} e^{\lambda_C t}.$$ (3.79)

Combining Eqs. (3.78) and (3.79), this continues until

$$\tau_C = \frac{1}{\lambda_C} \ln \left[\frac{J_{C,0}}{\gamma_C M_{R,0}} \right].$$ (3.80)

For $t > \tau_C$, there are enough ribosomes to balance all of the flux that the catabolic enzymes are capable of producing. Then the translational activity relaxes from the maximal value (γ_C) to the final steady state value (γ_f) according to Eq. (3.27).

3.5   Acknowledgments

Chapter 4

The simple model captures the kinetics of carbon upshift

4.1 Kinetic data

4.1.1 Mannose add lactose upshift

Wild-type NCM3722 cells were grown in N-C- medium with 0.4% mannose as the sole carbon source. At time zero 0.4% lactose was added to the culture. The model captures the kinetics this mannose add lactose upshift. The expression of the *lac* operon requires the presence of lactose so its expression is negligible before the addition of lactose to the medium. Since metabolism of lactose requires LacZ, lactose cannot be metabolized immediately upon its addition to the medium and there is no discontinuity in flux or translational activity. More precisely, we take $M_{C2}(t = 0) = 0$ so that $\gamma_0 = \gamma_i$ (from Eq. (3.30)) and there are no free parameters in the model. The only inputs to the model that are specific for this upshift are the steady state growth rate on 0.4% mannose alone ($\lambda_i = 0.4\,\mathrm{h}^{-1}$) and the steady state growth rate of the final condition ($\lambda_f = 0.95\,\mathrm{h}^{-1}$). The result of the model is plotted with the mannose add lactose data in Fig. 4.1.

Here we discuss the theoretical prediction of the translational activity which helps illuminate the kinetics of mass accumulation discussed next. Translational activity could be measured directly by measuring the protein production rate and taking the ratio with total ribosome mass. Throughout carbon upshift, translational activity has

Figure 4.1: Mannose add lactose upshift. Wild-type NCM3722 cells were grown in 0.4% mannose. At time zero, 0.4% lactose was added. The translational activity, OD600, flux, and growth rate are plotted as a function of time. The blue curves are the result of the model. The black data points are the data.

three regimes. In the first regime translational activity is constant during steady state growth on mannose (before the addition of lactose). During the second regime from the moment of lactose addition until ≈30min later, the translational activity increases and quickly approaches the translational activity of the final steady state condition. In the third regime the translational activity has reached its final steady state value.

Comparison of the total protein mass M of the model and the $OD600$ data reveals very good agreement. We look deeper into the data by taking derivatives.

Protein synthesis flux exhibits three regimes due to the three regimes of translational activity. Of course, protein synthesis flux is the product of translational activity and the mass of ribosomes. Before upshift, in the first regime, flux grows exponentially with rate equal to the steady state growth rate on mannose alone (λ_i =0.4 h^{-1}). In this regime translational activity is constant and ribosome mass increases exponentially with λ_i. In the second regime immediately after upshift, flux increases quickly over a short time. In this regime the translational activity is increasing and the production rate of ribosomes is increasing. The slow down in the rate of increase of flux coincides with the translational activity reaching its final value. In the final regime, flux grows exponentially with rate equal to the final steady state growth rate λ_f =0.95 h^{-1}. During this time the translational activity is constant and the mass of ribosomes increases exponentially with the final steady state growth rate.

Growth rate exhibits the same three regimes. In the first regime the culture is in steady state growth on mannose as the sole carbon source and the growth rate is constant. In the second regime the flux increases quickly and the growth rate also increases quickly. In the third regime the growth rate very slowly approaches the final steady state growth rate.

Thus the model is able to capture the kinetics of mass accumulation throughout the mannose add lactose upshift without a fit parameter. The only inputs to the model for this specific carbon upshift are the values of the steady state growth rates before and after the upshift.

In addition to the kinetics of mass accumulation, the model predicts the expression of the catabolic enzymes. The expression of the *lac* operon is measured directly by enzymatic assay of LacZ and compared to the model's prediction in Figure 4.2. The
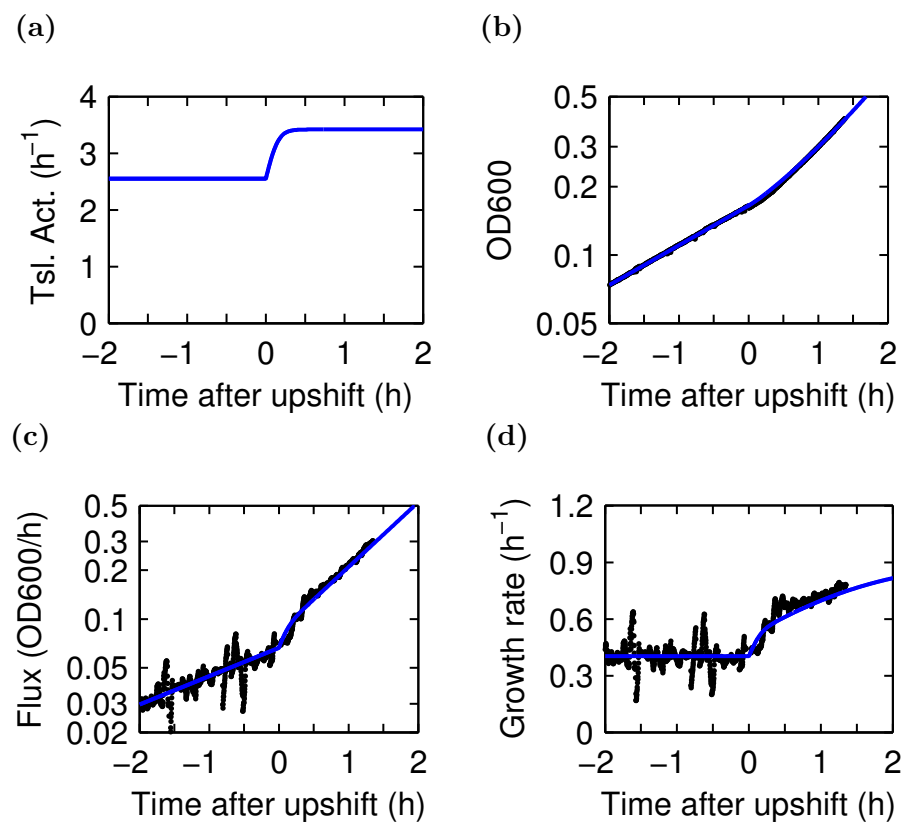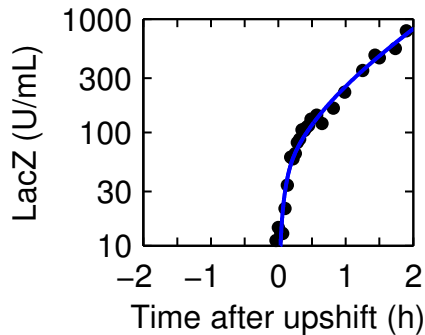
Figure 4.2: LacZ throughout the mannose add lactose upshift. Wild-type NCM3722 cells were grown in 0.4% mannose. At time zero, 0.4% lactose was added. LacZ was measured using an activity assay (black points). The blue curve is the result of the model. The raw LacZ data is presented in Table 7.5

model is able to capture the expression of LacZ. The only additional knowledge required is the expression of LacZ in steady state, which sets the proportionality factor of the y-axis.

4.1.2 Mannose add succinate upshift

NQ354 ($\Delta lacI$) was grown in N-C- medium with 0.1% mannose as the sole carbon source. At time zero 0.4% succinate was added to the culture. The model captures the kinetics of the mannose add succinate upshift by using the initial translational activity at the moment of its addition as a fit parameter (Fig. 4.3, blue solid curves). Succinate is known to be immediately taken up by *E. coli* when growing on glycolytic carbon sources [14]. The only other inputs to the model that are specific for this upshift are the steady state growth rate on 0.4% mannose alone (λ_i =0.19 h^{-1}) and the steady state growth rate of the final condition (λ_f =0.66 h^{-1}). For comparison the result of the model assuming that there is no immediate succinate flux at the instant of upshift is also plotted (Fig. 4.3, red dashed curves).

In order to capture the kinetics of upshift, translational activity is discontinuous at the instant of upshift. The initial succinate flux is so high that the translational activity jumps higher than the final steady state value. The translational activity relaxes down to the final steady state value on a timescale of ≈30min.

The model's prediction of total protein mass agrees well with the measured
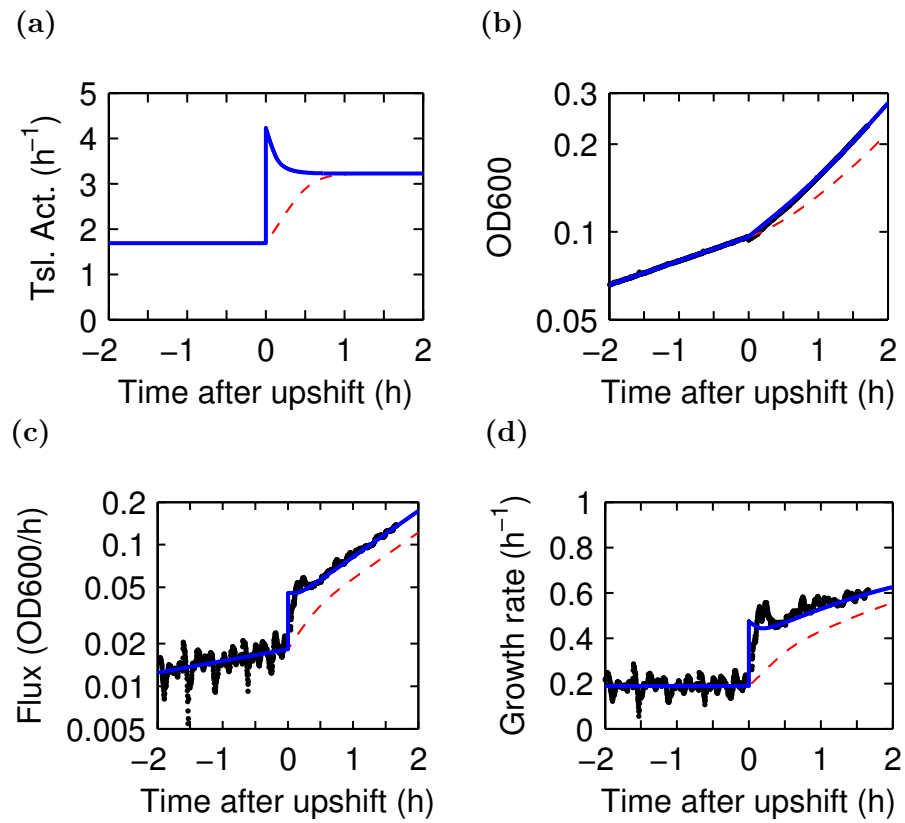
Figure 4.3: Mannose add succinate upshift. NQ354 ($\Delta lacI$) cells were grown in 0.1% mannose. At time zero, 0.4% succinate was added. The translational activity, OD600, flux, and growth rate are plotted as a function of time. The data is plotted as black points. The blue curves are the result of the model using γ_0 as a fit parameter. The red dashed curves are the result of the model that assumes there is no succinate flux at the instant of its addition $\gamma_0 = \gamma_i$.

OD600. The model that assumes no succinate flux at the instant of addition predicts that protein mass increases slower than the observed OD600.

Protein synthesis flux grows exponentially with the initial growth rate before the addition of succinate. When succinate is added flux increases immediately. Uptake of the added succinate must be immediate. Indeed, our model captures the kinetics of flux if we assume that the cell has some ability to uptake succinate at the instant of upshift and is unable to capture the kinetics otherwise. After the initial jump in flux, the rate of flux increase slows down as the translational activity decreases. As the translational activity reaches its final steady state value, flux increases exponentially with rate equal to the final steady state growth rate.

Growth rate is also captured by the model. The large increase in flux just after succinate addition is also observed as a roughly two fold increase in growth rate within the first few minutes after upshift. The model captures this nicely, as well as the ensuing slow relaxation to the final steady state growth rate.

Thus the model is able to capture the kinetics of mass accumulation throughout the mannose add succinate upshift. If the initial succinate flux is not accounted for, the model predicts slower kinetics of mass accumulation and is not consistent with the observations (red dashed curves in Figure 4.3).

In addition to the kinetics of mass accumulation, the model predicts the expression of catabolic enzymes. We cannot easily measure the expression of mannose or succinate enzymes so we instead use LacZ as a reporter of the expression of cAMP-dependent catabolic proteins. We use strain NQ354 ($\Delta lacI$) so that LacZ is expressed in the absence of lactose. Fig. 4.4 shows our observations along with the predictions of the model. The model captures the expression of LacZ throughout the upshift.

4.1.3 Mannose add OAA upshift.

NQ354 ($\Delta lacI$) cells were grown with 0.1% mannose as the sole carbon source. At time zero, 20mM OAA (oxaloacetic acid) was added. The flowcell data (black points) is plotted in Figure 4.5 along with the result of the model with $\gamma_0 = \gamma_i$ (red dashed curve) and with γ_0 used as a fit parameter (blue solid curve).

The increase in flux at the instant of OAA addition is very large; flux increases
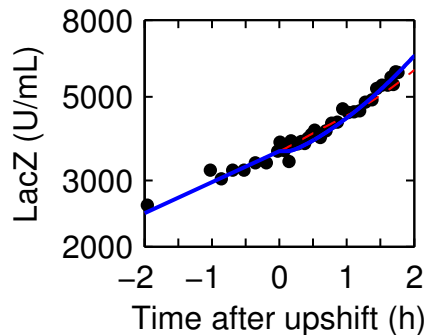
Figure 4.4: Mannose add succinate LacZ. NQ354 ($\Delta lacI$) cells were grown in 0.1% mannose. At time zero, 0.4% succinate was added. The LacZ activity is plotted as a function of time (black points; data in Table 7.6). The blue curve is the result of the model using γ_0 as a fit parameter. The red dashed curve is the result of the model that assumes there is no succinate flux at the instant of its addition $\gamma_0 = \gamma_i$.

roughly three fold in a matter of minutes. The kinetics of mass accumulation are only captured if the initial flux at the instant of upshift is used as a fit parameter. The sudden increase in flux is so large that the translational activity jumps to the maximum value allowed by the model. The translational activity remains maximal for several minutes before relaxing to the final steady state value.

The flux kinetics are well captured by the model. At the moment of upshift, flux immediately jumps to a high value with the translational activity. Flux then grows at a rate faster than the final steady state exponential rate because the translational activity is higher than in the final steady state and the ribosomes are predicted to accumulate at a rate higher than the final steady state rate (since their production rate is slaved to the translational activity in the model). Once the ribosome amount has increased enough relative to the carbon influx, the translational activity relaxes down to its final steady state value. After this the flux grows exponentially with rate equal to the final steady state growth rate.

The model also captures the kinetics of growth rate throughout the mannose add OAA upshift. The large increase in flux at the moment of upshift causes growth rate to increase a factor of three in just a few minutes. Thirty minutes later OD600 and flux have increased significantly, but growth rate has not increased. This is because the increasing translational capacity from having a higher ribosomal mass fraction is nearly

(a)

(b)

(c)

(d)
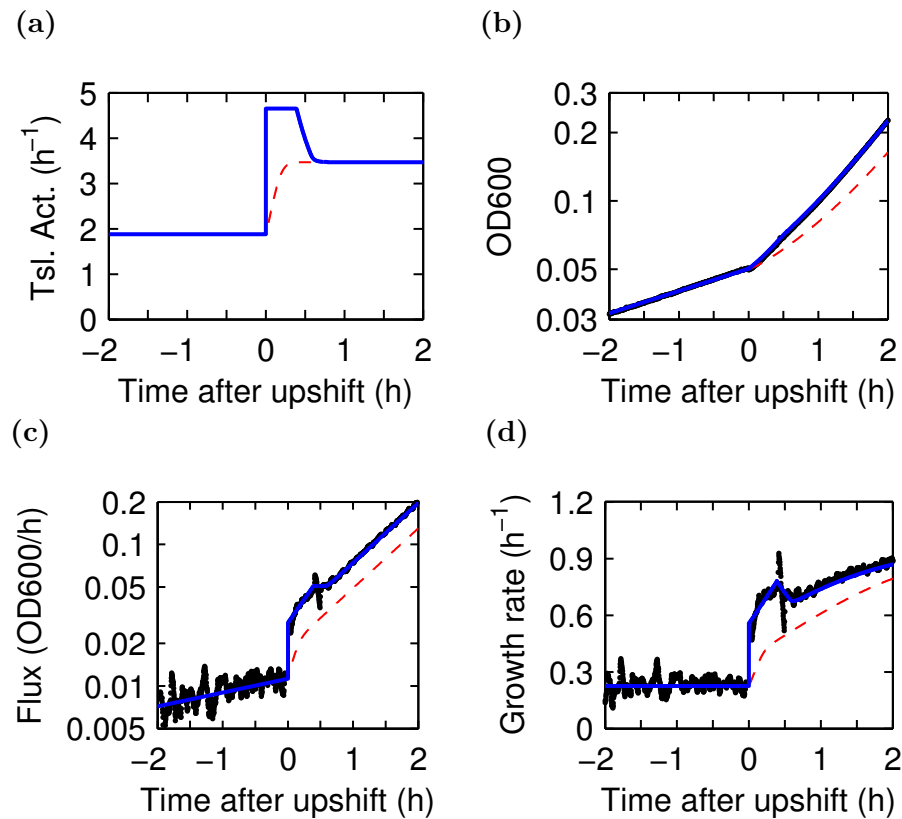
Figure 4.5: Mannose add OAA upshift. NQ354 ($\Delta lacI$) cells were grown in 0.1% mannose. At time zero, 20mM OAA was added. The translational activity, OD600, flux, and growth rate are plotted as a function of time. The data is plotted as black points. The blue curves are the result of the model using γ_0 as a fit parameter. The red dashed curves are the result of the model that assumes there is no OAA flux at the instant of its addition $\gamma_0 = \gamma_i$. The model uses the initial and final growth rates $\lambda_i = 0.22\,\mathrm{h}^{-1}$ and $\lambda_f = 0.97\,\mathrm{h}^{-1}$, respectively.
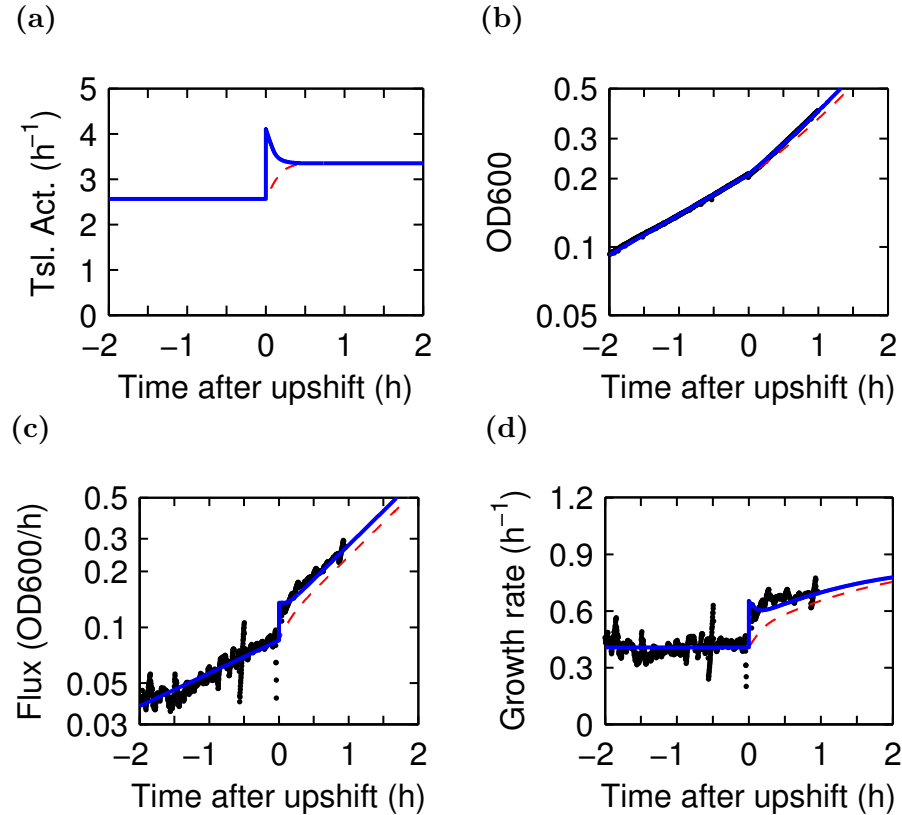
Figure 4.6: Mannose add glucose upshift. Wild-type NCM3722 cells were grown in 0.4% mannose. At time zero, 0.4% glucose was added. The translational activity, OD600, flux, and growth rate are plotted as a function of time. The data is plotted as black points. The blue curves are the result of the model using γ_0 as a fit parameter. The red dashed curves are the result of the model that assumes there is no glucose flux at the instant of its addition $\gamma_0 = \gamma_i$.

balanced by the decrease in translational activity.

4.1.4 Mannose add glucose upshift.

Wild-type NCM3722 cells were grown in 0.4% mannose. At time zero, 0.4% glucose was added. Flowcell data (black points), the model using the initial glucose flux as a fit parameter (blue solid curve), and model assuming no initial glucose flux (red dashed curve) are plotted in Figure 4.6.

Initially the culture is in steady state exponential growth on 0.4% mannose as the sole carbon source. OD600 and flux increase exponentially with rate equal to the initial steady state growth rate; growth rate is constant at this value. Growth rate and

flux increase very quickly at the instant of glucose addition, implying that the uptake of glucose must be immediate. Using the initial glucose flux as a fit parameter we find excellent agreement with our model. Just after upshift, flux initially increases more quickly than it does in final steady state. The ribosome amount cannot change much on this timescale so the translational activity increases to balance flux. As the translational activity relaxes to its final steady state value, flux grows exponentially with the final steady state growth rate and growth rate asymptotically approaches its final steady state value.

4.1.5   Mannose add glycerol upshift.

Wild-type NCM3722 cells were grown in $100\,\mu$M IPTG and 0.4% mannose. At time zero, 0.4% glycerol was added. Figure 4.7 shows flowcell data (black points) along with the result of the model using the initial glycerol flux as a fit parameter (blue solid curves). For reference the model result assuming that glycerol cannot immediately be incorporated by the cell is shown as red dashed curves.

For this upshift the model is again able to capture the kinetics of mass accumulation. The model suggests that glycerol is able to be taken up by the cell immediately upon being added to the culture. This is consistent with the large increase in flux and growth rate just after the addition of glycerol. About 30min after the upshift the rate of flux increase slows down and increases exponentially with rate equal to the final steady state growth rate. Growth rate also increases at a slower rate and asymptotically approaches the final steady state growth rate.

(a)

(b)

(c)

(d)
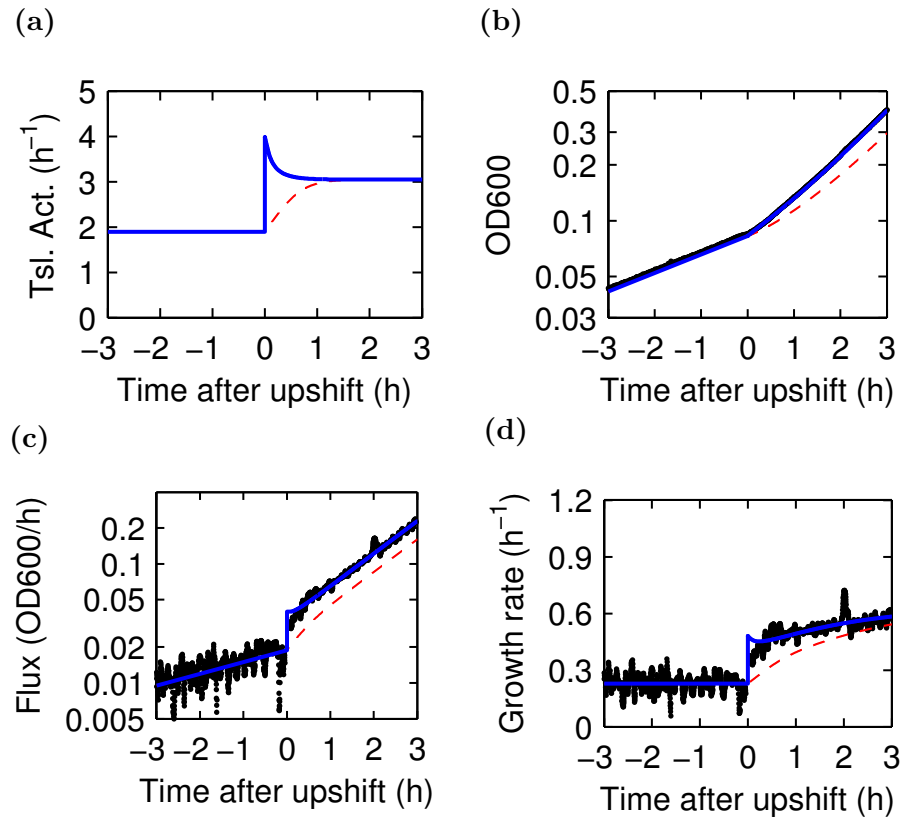
Figure 4.7: Mannose add glycerol upshift. Wild-type NCM3722 cells were grown in $100\,\mu$M IPTG and 0.4% mannose. At time zero, 0.4% glycerol was added. The translational activity, OD600, flux, and growth rate are plotted as a function of time. The data is plotted as black points. The blue curves are the result of the model using γ_0 as a fit parameter. The red dashed curves are the result of the model that assumes there is no glycerol flux at the instant of its addition $\gamma_0 = \gamma_i$.

4.2   Direct titration of flux at the instant of upshift

We have thus far observed that the model is capable of reproducing kinetic data if we use the initial carbon uptake at the instant of addition as a fit parameter. To directly test the effect of varying levels of initial carbon uptake on the kinetics of mass accumulation, we constructed a strain with inducible expression of the succinate transporter. We repeat the mannose add succinate upshift that was studied above, but now with various levels of initial succinate uptake set synthetically. We find novel, interesting upshift kinetics and find that our model reproduces the kinetics of upshift using the initial carbon uptake as a fit parameter.

Strain NQ530 has the native *dctA* promoter replaced with the inducible promoter *Pu* [36]. The *Pu* promoter requires activation by the transcription factor XylR so we drive the *xylR* gene with the synthetic *lac* promoter $P_{Llac-O1}$ (a promoter that is repressed by LacI but does not need Crp-cAMP for activation) at the *attB* chromosomal site. We use 100 μM IPTG is used to induce expression of XylR. The transcription factor XylR requires activation by an inducer to activate the *Pu* promoter. We use various concentrations of the inducer 3-methylbenzyl alcohol (3MBA) to induce various levels of DctA expression.

We culture strain NQ530 in minimal medium with 0.1%mannose as the sole carbon source. To titrate the level of DctA expression, we use 100 μM IPTG to induce XylR and various concentrations (0, 32, 64 μM) of the inducer 3MBA. During steady state balanced growth in these conditions, succinate is added to a final concentration of 20 mM. Thus the bacteria experience a carbon upshift with various uptake levels at the instant of upshift. At the moment of upshift, we also add 3MBA in the appropriate amount so that all cultures have the same final concentration of 64 μM and thus also have the same final growth rate.

There is a sudden increase in flux just after upshift. The size of the increase correlates with the expression of DctA at the moment of upshift. This makes intuitive sense and confirms our hypothesis that increasing the uptake rate of the upshift carbon affects the kinetics of mass accumulation after upshift. Not long after upshift, flux increases exponentially with rate equal to the final growth rate so that the flux of each culture is parallel. The cultures that had higher flux at the moment of upshift always

(a)

(b)
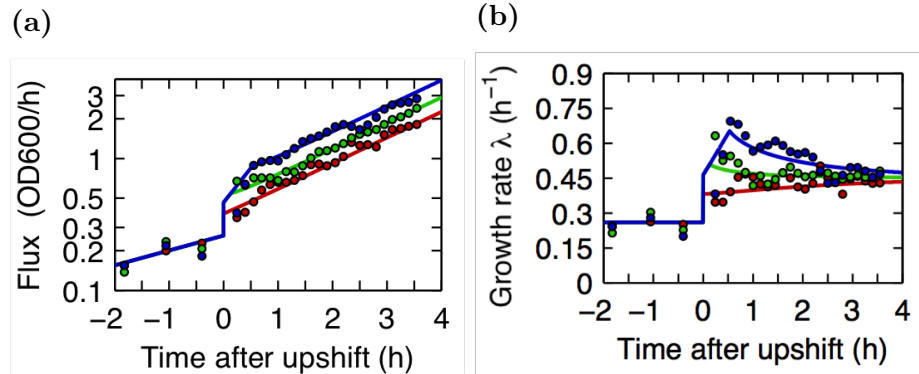
Figure 4.8: Direct titration of initial carbon flux. NQ530 cells were grown in 0.1%mannose with $100\,\mu M$ IPTG and 0, 32, or $64\,\mu M$ 3MBA (red, green, blue points, respectively). At time zero $20\,mM$ succinate is added to the cultures. Simultaneously, 3MBA is added so that all cultures have the same final concentration of $64\,\mu M$. We plot the observed flux and growth rate. The raw OD600 data is available in Table 7.7.

maintain their advantage. The model (plotted as curves with the same color scheme as the points) is able to capture the flux of all cultures by using the initial carbon flux as a fit parameter.

Growth rate, like flux, has a quick increase at the moment of upshift that correlates with the expression level of DctA. Amazingly, *growth rate overshoots the final steady state value* for the highest levels of DctA expression. Growth rate slowly relaxes down to the steady state value, but the relaxation takes hours. The slow downward relaxation of growth rate is reminiscent of the slow upward relaxation in a typical upshift. Our simple model reproduces the kinetics of growth rate, including the overshoot of the final steady state growth rate.

We briefly discuss how it is possible for the growth rate to overshoot the final steady state value. When we discussed the long timescale of growth rate relaxation from below we noted that it results from the presence of unwanted proteins left over from the cell's history. When growth rate overshoots the final value, it means that the cell transiently uses its mass more efficiently for cell growth than it does in the final steady state. The model suggests that this is because the cell has transiently accumulated a higher ribosomal mass fraction than the final steady state $(\phi_R(t) > \phi_{R,f})$. The high ribosomal mass fraction comes at the cost of the mass fraction of other (non-flux-producing) proteins. This happens as a result of the high initial carbon flux. To

handle the high flux, the cell produces so many ribosomes that the ribosomal mass fraction exceeds the final steady state mass fraction.

4.3   Acknowledgments

With permission from the coauthors, all chapters of this dissertation contain work from a manuscript that is in preparation with the working title "A quantitative theory for the kinetics of bacterial growth transition" 2014, D. W. Erickson, S. Schink, U. Gerland, and T. Hwa.

Chapter 5

Extension of the simple analytical model to carbon downshift

5.1 Introduction

In this chapter we extend the model developed for carbon upshift in Chapter 3 to the realm of carbon downshifts. We consider "carbon downshifts" in which *E. coli* is cultured in minimal medium in the presence of two simultaneously used carbon sources at 37°C. The concentration of one of the carbon sources is chosen such that it is exhausted by cell growth. Then the culture transitions from steady state balanced growth on the combination of two carbon source to a new steady state balanced growth on only one of those carbon sources. The final steady state growth rate is slower than the initial steady state growth rate.

5.2 Model

Here we derive our model for carbon downshift. The model is analagous to the carbon upshift model developed in Chapter 3.

As in Eq. (3.1), protein synthesis flux is defined as the rate of increase of protein mass

$$J_R \equiv \frac{dM}{dt}. \qquad (5.1)$$

Protein synthesis is again given by

$$\frac{d}{dt}M_R = \chi_R(t) \cdot J_R(t), \tag{5.2}$$

$$\frac{d}{dt}M_{C1} = H_{C1}(t) \cdot \chi_C(t) \cdot J_R(t), \tag{5.3}$$

$$\frac{d}{dt}M_{C2} = H_{C2}(t) \cdot \chi_C(t) \cdot J_R(t), \tag{5.4}$$

as in Eqs. (3.2)-(3.4). $\chi_R(t)$ and $\chi_C(t)$ summarize the regulation of ribosomal proteins (M_R) and the catabolic enzymes (M_{C1} and M_{C2}), respectively. $H_{C1}(t)$ and $H_{C2}(t)$ are the self-regulatory functions. We consider carbon downshifts where carbon source $C1$ is exhausted by cell growth. We take $H_{C1}(t) = h_{C1}$ constant for all time and $H_{C2}(t) = h_{C2}$ constant for all time. The values of the constants are not important as they can be absorbed into k_{C1} and k_{C2} below.

As before, to keep the description contained within the essential dynamical variables introduced above, we define translational activity as

$$\gamma \equiv \frac{J_R}{M_R}, \tag{5.5}$$

and note that it reflects the levels of tRNA charging and carbon precursors.

We again make the Ansatz that $\chi_R(t)$ and $\chi_C(t)$ depend on time only through $\gamma(t)$ so that

$$\chi_R(t) = f_R(\gamma(t)) = \frac{\lambda_f}{\gamma_f}\left(\frac{1 - \gamma_f/\gamma_{\max}}{1 - \gamma(t)/\gamma_{\max}}\right), \tag{5.6}$$

$$\chi_C(t) = f_C(\gamma(t)) = 1 - \frac{\lambda_f}{\lambda_C}\frac{\gamma(t)}{\gamma_f}\left(\frac{1 - \gamma_f/\gamma_{\max}}{1 - \gamma(t)/\gamma_{\max}}\right) = 1 - \frac{\gamma(t)}{\lambda_C}\chi_R(t). \tag{5.7}$$

Catabolic proteins determine the carbon flux

$$J_C(t) = K_{C1}(t)M_{C1} + K_{C2}(t)M_{C2}. \tag{5.8}$$

$K_{C1}(t)$ and $K_{C2}(t)$ are the catabolic rate functions. $C2$ is present in saturating concentrations for all time so $K_{C2}(t) = k_{C2}$ is constant for all time. $C1$ is depleted by cell growth so its concentration decreases in time and its catabolic rate function is a

Michaelis function of $C1$ concentration

$$K_{C1}(t) = k_{C1}\frac{[C1](t)}{k_{m,C1} + [C1](t)}, \tag{5.9}$$

with rate constant k_{C1}, Michaelis constant $k_{m,C1}$, and time-dependent $C1$ concentration $[C1](t)$. The concentration of $C1$ in the medium decreases as a result of metabolic flux

$$\frac{d}{dt}[C1] = -K_{C1}(t)M_{C1}(t). \tag{5.10}$$

Flux changes on a much faster timescale than protein mass, and thus we assume instantaneous flux balance to prevent the buildup of intermediate metabolites, *i.e.*,

$$J(t) \equiv J_R(t) = J_C(t). \tag{5.11}$$

Equations (5.1)-(5.11) completely define the dynamics of carbon downshift. The equations are more complicated than those for carbon upshift and they do not simplify as nicely. However, the equations are easily numerically integrated to obtain the kinetics of the growth transition.

5.3 The model simplifies after complete carbon exhaustion

Carbon $C1$ is completely depleted after time τ_{C1}

$$[C1](t > \tau_{C1}) = 0 \tag{5.12}$$

and the model simplifies greatly. The content of this section only considers this simplified regime. Then, from Eqs. (5.9) and (5.8), $C1$ no longer contributes to flux so that

$$J_C(t > \tau_{C1}) = k_{C2}M_{C2}. \tag{5.13}$$

Using the definition of translational activity in Eq. (5.5), the flux in Eq. (5.13), and protein synthesis kinetics in Eqs. (5.2) and (5.4) we find

$$\frac{d}{dt}\gamma = \gamma(t)\left[h_{C2}k_{C2}\chi_C(t) - \gamma(t)\chi_R(t)\right] \qquad (t > \tau_{C1}), \qquad (5.14)$$

a closed equation for $\gamma(t)$. *Equation (5.14) is of the same form as the differential equation Eq. (3.27) for translational activity in carbon upshift.* From the solution for $\gamma(t)$, we can obtain $M_R(t)$ from Eq. (5.2), or equivalently,

$$\frac{d}{dt}\ln\left(M_R\right) = \chi_R(t)\cdot\gamma(t). \qquad (5.15)$$

The flux $J_R(t)$ is finally obtained from $\gamma(t)$ and $M_R(t)$ via Eq. (5.5), and the growth curve $M(t)$ is obtained from $J_R(t)$ via Eq. (5.1).

We solve Eq. (5.14) in steady state using Eqs. (5.6) and (5.7) to find the constraint

$$T_d^{-1} \equiv h_{C2}k_{C2} = \frac{\lambda_f}{1 - \lambda_f/\lambda_C}, \qquad (5.16)$$

where, as above, λ_f is the final steady state growth rate and this downshift-affiliated timescale is defined to be T_d.

We rearrange Eq. (5.14) using Eqs. (5.6), (5.7) and (5.16)

$$dt = d\gamma\frac{T_d}{\gamma(t)}\left(\frac{1 - \gamma(t)/\gamma_{\max}}{1 - \gamma(t)/\gamma_f}\right) \qquad (5.17)$$

and integrate from time $t\tau_{C1}$ to time t to find

$$t = \tau_{C1} + T_d\ln\left[\left(\frac{\gamma(t)}{\gamma_{\tau C1}}\right)\left(\frac{1 - \gamma_{\tau C1}/\gamma_f}{1 - \gamma(t)/\gamma_f}\right)^{1-\gamma_f/\gamma_{\max}}\right], \qquad (5.18)$$

where $\gamma_{\tau C1}$ is the value of the translational activity at $t = \tau_{C1}$.

We integrate Eq. (5.14) directly using Eq. (5.17) to find

$$M_R(\gamma) = M_{R,\tau C1}\left(\frac{1 - \gamma_{\tau C1}/\gamma_f}{1 - \gamma(t)/\gamma_f}\right)^{(1-\lambda_f/\lambda_C)(1-\gamma_f/\gamma_{\max})}, \qquad (5.19)$$

where $M_{R,\tau C1} \equiv M_R(t = \tau_{C1})$. Then, from Eq. (5.5),

$$J(\gamma) = M_{R,\tau C1}\gamma(t)\left(\frac{1 - \gamma_{\tau C1}/\gamma_f}{1 - \gamma(t)/\gamma_f}\right)^{(1-\lambda_f/\lambda_C)(1-\gamma_f/\gamma_{\max})}. \quad (5.20)$$

We simplify these expressions using Eq. (5.18) and find

$$M_R(t) = M_{R,\tau C1}\left(\frac{\gamma_{\tau C1}}{\gamma(t)}\right)^{1-\lambda_f/\lambda_C} e^{\lambda_f(t-\tau_{C1})} \quad (5.21)$$

and

$$J(t) = J_{\tau C1}\left(\frac{\gamma(t)}{\gamma_{\tau C1}}\right)^{\lambda_f/\lambda_C} e^{\lambda_f(t-\tau_{C1})}, \quad (5.22)$$

where

$$J_{\tau C1} \equiv J(t = \tau_{C1}) = \gamma_{\tau C1}M_{R,\tau C1} \quad (5.23)$$

in accordance with Eq. (5.5). We determine the kinetics of the growth curve $M(t)$ by integrating Eq. (5.1) directly using Eqs. (5.17) and (5.20) and simplify the result using Eq. (5.16)

$$M(\gamma(t)) = M_{\tau C1} - M_{R,\tau C1}\left(\frac{\gamma_f}{\lambda_f}\right)\left(\frac{1 + T_d\lambda_C\gamma_{\tau C1}/\gamma_{\max}}{1 + T_d\lambda_C\gamma_f/\gamma_{\max}}\right) \quad (5.24)$$
$$+ M_{R,\tau C1}\left(\frac{\gamma_f}{\lambda_f}\right)\left(\frac{1 + T_d\lambda_C\gamma(t)/\gamma_{\max}}{1 + T_d\lambda_C\gamma_f/\gamma_{\max}}\right)\left(\frac{1 - \gamma_{\tau C1}/\gamma_f}{1 - \gamma(t)/\gamma_f}\right)^{\left(1-\frac{\lambda_f}{\lambda_C}\right)\left(1-\frac{\gamma_f}{\gamma_{\max}}\right)},$$

where $M_{\tau C1}$ is the total protein mass at the time when $C1$ is exhausted.

We calculate the exact form of the growth rate λ using its definition Eq. (3.7) and Eqs. (5.20) and (5.24)

$$\lambda\left(\gamma(t)\right) = \lambda_f \frac{\left(\frac{\gamma(t)}{\gamma_f}\right)\left(\frac{1-\gamma_{\tau C1}/\gamma_f}{1-\gamma(t)/\gamma_f}\right)^{(1-\lambda_f/\lambda_C)(1-\gamma_f/\gamma_{\max})}}{\left(\frac{M_{\tau C1}}{M_{R,\tau C1}}\right)\left(\frac{\lambda_f}{\gamma_f}\right) - \left(\frac{1+T_d\lambda_C\gamma_{\tau C1}/\gamma_{\max}}{1+T_d\lambda_C\gamma_f/\gamma_{\max}}\right)}{+ \left(\frac{1+T_d\lambda_C\gamma(t)/\gamma_{\max}}{1+T_d\lambda_C\gamma_f/\gamma_{\max}}\right)\left(\frac{1-\gamma_{\tau C1}/\gamma_f}{1-\gamma(t)/\gamma_f}\right)^{\left(1-\frac{\lambda_f}{\lambda_C}\right)\left(1-\frac{\gamma_f}{\gamma_{\max}}\right)}}. \quad (5.25)$$

These calculations reveal the exact solutions of flux, protein mass, and growth rate throughout downshift after one of the original carbon sources has been completely exhausted. Note that $C1_0$ and $k_{m,C1}$ do not appear. Instead, the solutions require

the values of translational activity, total ribosome mass, and total protein mass at the time when $C1$ is completely exhausted, which are determined by $C1_0$ and $k_{m,C1}$. For carbon upshift, the "initial conditions" (at the moment of upshift) of these parameters were known from the initial steady state condition and the mass of upshift. For carbon downshift, this does not strictly apply because the cell responds to the decreasing concentration of the carbon source that is being exhausted. However, the values can be computed by calculating the exact solution of the full model. In addition, if $k_{m,C1}$ is small relative to the initial $C1$ concentration, the change in carbon concentration happens very quickly so that the cell does not have much time to respond. In this case the "initial conditions" are approximately equal to the initial steady state values.

Once carbon C1 is completely depleted, the kinetics of translational activity are of the same form as for carbon upshift transitions (compare Equations (5.18) and (3.35)). The kinetics of protein synthesis flux are also the same for the two transitions (compare Equations (5.20) and (3.44)). However, the proteome composition is different for these two types of transitions, and thus the fraction of the proteome contributing to growth is different. Thus the kinetics of protein mass and of instantaneous growth rate are different for carbon downshift and carbon upshift.

5.4   Downshift kinetic data

In this section we explore the kinetics of carbon downshift. We compare our observations to the numerical solution of the full downshift model developed in Section 5.2. Numerical solution of the model requires four parameters specific to each downshift: the initial steady state growth rate λ_i, the final steady state growth rate λ_f, the initial concentration of the carbon that is depleted $C1_0$ (and the carbon yield relating this carbon concentration to the amount of biomass produced), and the Michaelis constant of the rate-limiting enzyme responsible for the metabolism of the depleted carbon $k_{m,C1}$. The known initial carbon concentration $C1_0$ sets the OD600 at which the downshift occurs. The Michaelis constant $k_{m,C1}$ determines how quick the downshift is and influences how much the various quantities (*e.g.* flux, growth rate) decrease as the carbon is exhausted. k_{mC1} is the only parameter that cannot be measured and we thus use it as a fit parame-
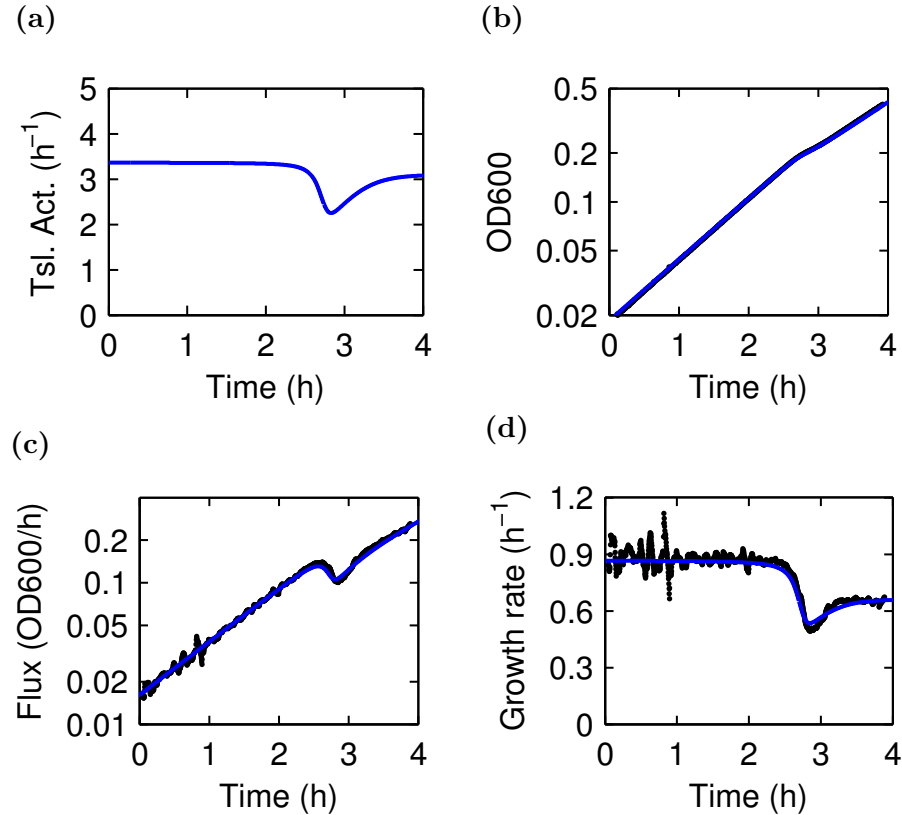
Figure 5.1: Pyruvate with OAA depletion downshift. NQ354 ($\Delta lacI$) cells were grown in the combination of OAA and pyruvate. OAA concentration was chosen such that OAA was exhausted during growth. The translational activity, OD600, flux, and growth rate are plotted as a function of time. The blue curves are the result of the model. The black data points are the data.

ter. As noted in Section 5.3, the kinetics of growth recovery after $C1$ exhaustion do not depend on $C1_0$ or $k_{m,C1}$.

5.4.1 Pyruvate with OAA depletion

NQ354 ($\Delta lacI$) cells were grown in the combination of OAA and pyruvate. OAA concentration was chosen such that OAA was exhausted during growth. The model is able to capture the kinetics of this pyruvate with OAA depletion downshift. The kinetic data (black points) and the result of the model (blue curves) are shown in Figure 5.1. The inputs to the model are the initial growth rate $\lambda_i=0.88\,\mathrm{h}^{-1}$, the final growth rate $\lambda_f=0.66\,\mathrm{h}^{-1}$, the initial OAA concentration 0.095 OD600, and the Michaelis constant of

the rate-limiting OAA catabolic enzyme $k_{m,C1}$=0.005 OD600. The exact OAA concentration in mM at the time of downshift is unknown because in solution OAA unstable and spontaneously decarboxylates to pyruvate [37].

Initially the culture is in steady state exponential growth. OD and flux increase exponentially with rate equal to the steady state growth rate; growth rate is constant in time and also equal to the steady state growth rate. During this time translational activity is constant at the steady state value of the initial culture. At OD600 $\approx$ 0.2 OAA is exhausted and the exponential growth of OD600 is interrupted by a lag followed by a slower rate of increase. The depletion of OAA causes influx of OAA to decrease. As a result protein synthesis flux decreases, deviating from its exponentially increasing behavior. The ribosomal protein mass does not significantly change during this time and the translational activity decreases along with flux. During this time the growth rate decreases from λ_i= $0.88\,\mathrm{h}^{-1}$ to about $0.5\,\mathrm{h}^{-1}$, reflecting a decrease in flux of about 50%.

Protein synthesis flux quickly begins increasing again as pyruvate flux takes over as the dominant carbon flux. The translational activity begins to increase as well, but is below the final steady state value. Thus the cell has a high catabolic protein synthesis rate and a small ribosomal protein synthesis rate, relative to the final steady state. Since the cell is able to invest a higher fraction of protein synthesis towards the flux-limiting catabolic proteins, flux transiently increases more quickly than the final steady state growth rate. As the stoichiometry of the flux producing catabolic enzymes and the flux consuming ribosomal proteins reaches the final steady state levels, the translational activity relaxes to its final steady state value and flux grows exponentially with the final steady state growth rate. Likewise, growth rate stabilizes at its constant final steady state value.

5.4.2 Pyruvate with gluconate depletion

Wild-type NCM3722 cells were grown in the presence of 1mM IPTG with 20mM pyruvate and 5.6mM gluconate as the only carbon sources. Pyruvate is always present in saturating concentrations, but gluconate is exhausted just before the OD600 reaches 0.2. The model is able to capture the kinetics of this pyruvate with gluconate depletion carbon downshift. The kinetic data (black points) and the result of the model (blue

(a)

(b)

(c)

(d)

Figure 5.2: Pyruvate with gluconate depletion downshift. Wild-type NCM3722 cells were grown in the presence of 1mM IPTG. The only carbon sources are 20mM pyruvate and 5.6mM gluconate. Pyruvate is always metabolized by the culture, but gluconate is exhausted during growth and the culture transitions to slower growth. The translational activity, OD600, flux, and growth rate are plotted as a function of time. The blue curves are the result of the model. The black data points are the data. The OD600 data is available in Table 7.8.

curves) are shown in Figure 5.2. Here the data was taken by hand in batch culture. The derivatives (flux and growth rate) were calculated as the slope of a best-fit line over a sliding window of three consecutive OD600 measurements. The inputs to the model are the initial growth rate $\lambda_i=1.01\,\mathrm{h}^{-1}$, the final growth rate $\lambda_f=0.7\,\mathrm{h}^{-1}$, the initial gluconate concentration (0.11 OD600), and the Michaelis constant of the rate-limiting gluconate catabolic enzyme $k_{m,C1}=0.007$ OD600.

Initially the culture is in steady state exponential growth on the combination of pyruvate and gluconate. OD and flux increase exponentially with rate equal to the initial steady state growth rate. Growth rate is constant in time and also equal to the

steady state growth rate. During this time translational activity is constant at the steady state value of the initial culture. Before OD600 reaches 0.2, gluconate is exhausted and the exponential growth of OD600 is interrupted by a lag followed by a slower rate of increase. Protein synthesis flux decreases, deviating from its exponentially increasing behavior. The ribosomal protein mass does not significantly change during this time and the translational activity decreases along with flux. During this time the growth rate decreases from $\lambda_i = 1.01 \, \mathrm{h}^{-1}$ to about $0.4 \, \mathrm{h}^{-1}$, reflecting a decrease in flux of about 40%.

Protein synthesis flux quickly begins increasing again as pyruvate flux takes over as the dominant carbon flux. The translational activity begins to increase as well, but is below the final steady state value. Thus the cell has a high catabolic protein synthesis rate and a small ribosomal protein synthesis rate, relative to the final steady state. Since the cell is able to invest a higher fraction of protein synthesis towards the flux-limiting catabolic proteins, flux transiently increases more quickly than the final steady state growth rate. As the stoichiometry of the flux producing catabolic enzymes and the flux consuming ribosomal proteins reaches the final steady state levels, the translational activity relaxes to its final steady state value and flux grows exponentially with the final steady state growth rate. Likewise, growth rate stabilizes at its constant final steady state value.

5.4.3   Succinate with gluconate depletion

Wild-type NCM3722 cells were grown in the presence of 1mM IPTG with 20mM succinate and 5.6mM gluconate as the only carbon sources. Succinate is always present in saturating concentrations, but gluconate is exhausted just after the OD600 reaches 0.1. Gluconate is exhausted at a lower OD600 in this downshift than in the pyruvate with gluconate depletion downshift because gluconate makes up a higher fraction of the total carbon flux when the culture is grown on the combination of succinate and gluconate. The model is able to capture the kinetics of this succinate with gluconate depletion carbon downshift. The kinetic data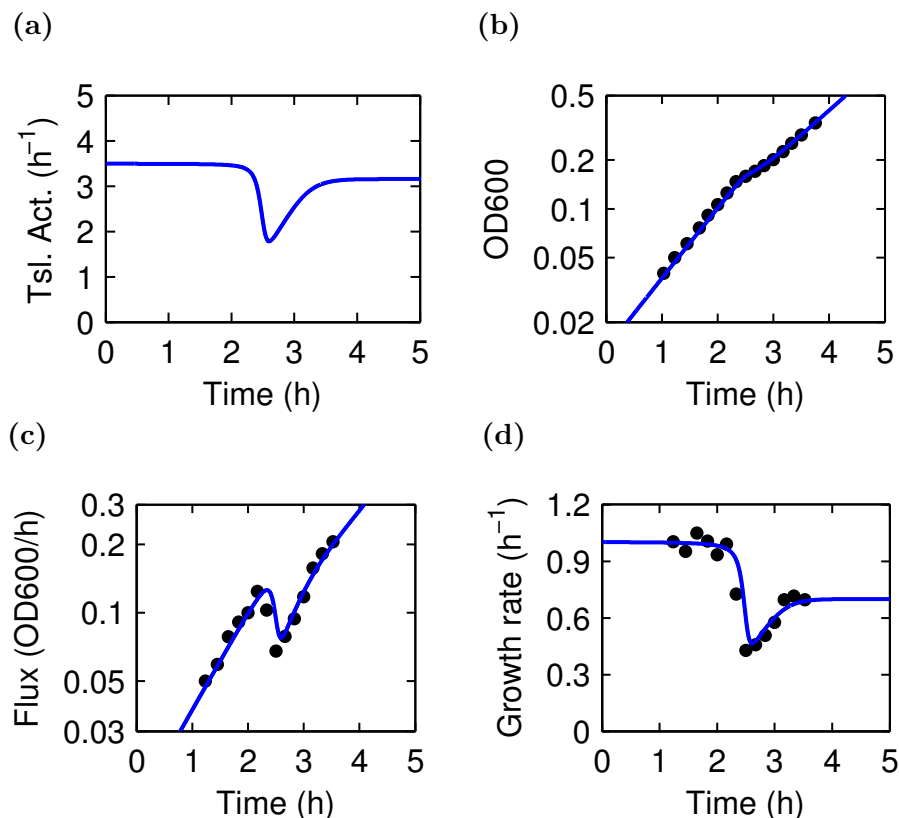 (black points) and the result of the model (blue curves) are shown in Figure 5.3. Here the data was taken by hand in batch culture. The derivatives (flux and growth rate) were calculated as the slope of a best-fit line

Figure 5.3: Succinate with gluconate depletion downshift. Wild-type NCM3722 cells were grown in the presence of 1mM IPTG with 20mM succinate and 5.6mM gluconate as carbon sources. Succinate is always present and metabolized by the culture, but gluconate is exhausted during growth and the culture transitions to slower growth. The translational activity, OD600, flux, and growth rate are plotted as a function of time. The blue curves are the result of the model. The black data points are the data. The raw OD600 data is reported in Table 7.9.

over a sliding window of three consecutive OD600 measurements. The inputs to the model are the initial growth rate λ_i=0.90 h^{-1}, the final growth rate λ_f=0.46 h^{-1}, the initial gluconate concentration (0.085 OD600), and the Michaelis constant of the rate-limiting gluconate catabolic enzyme $k_{m,C1}$=0.007 OD600 (the same value used for the other pyruvate with gluconate depletion downshift).

Initially the culture is in steady state exponential growth on the combination of succinate and gluconate. OD and flux increase exponentially with rate equal to the initial steady state growth rate. Growth rate is constant in time and also equal to the steady state growth rate. During this time translational activity is constant at the steady

state value of the initial culture. Just after OD600 reaches 0.1, gluconate is exhausted and the exponential growth of OD600 is interrupted by a lag followed by a slower rate of increase. Protein synthesis flux decreases, deviating from its exponentially increasing behavior. The ribosomal protein mass does not significantly change during this time and the translational activity decreases along with flux. During this time the growth rate decreases from $\lambda_i = 0.90\,\text{h}^{-1}$ to about $0.3\,\text{h}^{-1}$, reflecting a decrease in flux of about a third.

Protein synthesis flux quickly begins increasing again as succinate flux takes over as the dominant carbon flux. The translational activity begins to increase as well, but is below the final steady state value. Thus the cell has a high catabolic protein synthesis rate and a small ribosomal protein synthesis rate, relative to the final steady state. Since the cell is able to invest a higher fraction of protein synthesis towards the flux-limiting catabolic proteins, flux transiently increases more quickly than the final steady state growth rate. As the stoichiometry of the flux producing catabolic enzymes and the flux consuming ribosomal proteins reaches the final steady state levels, the translational activity relaxes to its final steady state value and flux grows exponentially with the final steady state growth rate. Likewise, growth rate stabilizes at its constant final steady state value.

5.4.4 Succinate with glucose depletion

Wild-type NCM3722 cells were grown in the presence of 0.4% succinate and 0.5mM glucose as the only carbon sources. Succinate is always present in saturating concentrations, but glucose is exhausted at about 0.1 OD600. The model is able to capture the kinetics of this succinate with glucose depletion carbon downshift. The kinetic data (black points) and the result of the model (blue curves) are shown in Figure 5.4. Here the data was taken by hand in batch culture. The derivatives (flux and growth rate) wer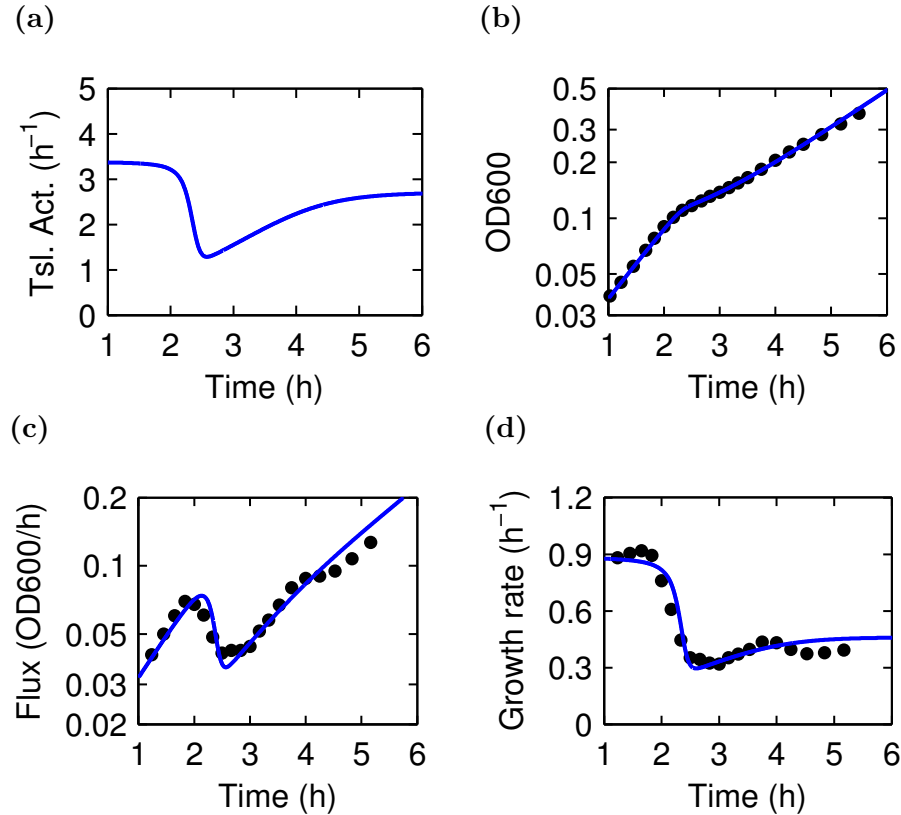e calculated as the slope of a best-fit line over a sliding window of three consecutive OD600 measurements. The inputs to the model are the initial growth rate $\lambda_i = 1.08\,\text{h}^{-1}$, the final growth rate $\lambda_f = 0.66\,\text{h}^{-1}$, the initial glucose concentration (0.07 OD600), and the Michaelis constant of the rate-limiting glucose catabolic enzyme $k_{m,C1} = 0.002$ OD600.

Initially the culture is in steady state exponential growth on the combination
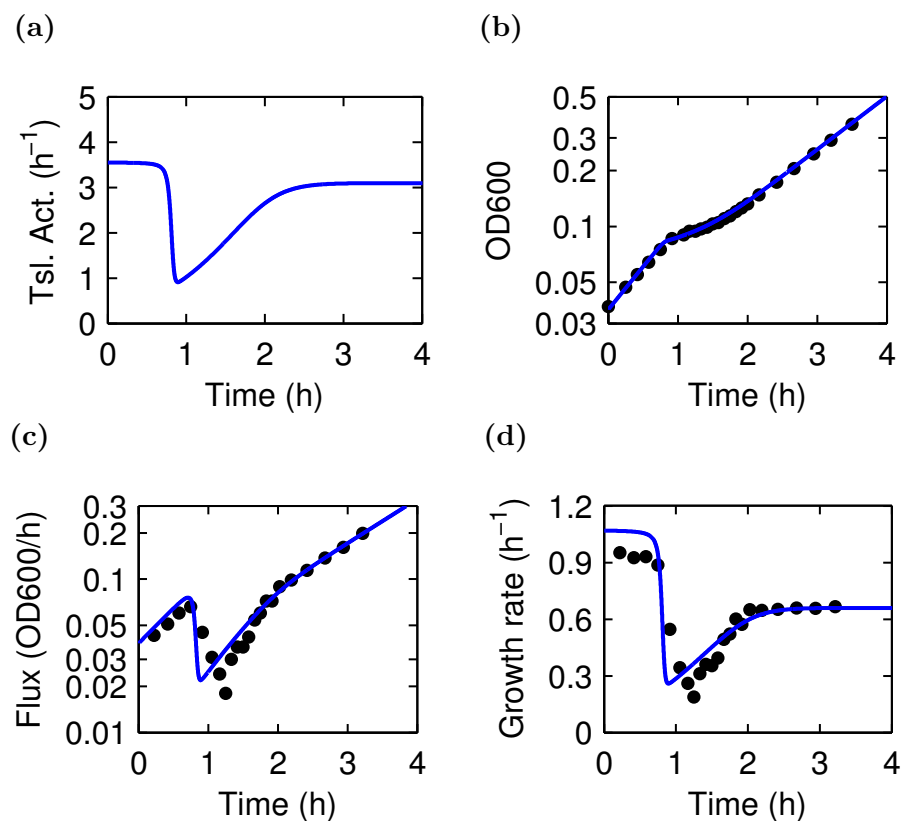
Figure 5.4: Succinate with glucose depletion downshift. Wild-type NCM3722 cells were grown on 0.4% succinate and 0.5mM glucose as the only carbon sources. Succinate is always present and metabolized by the culture, but glucose is exhausted during growth and the culture transitions to slower growth. The translational activity, OD600, flux, and growth rate are plotted as a function of time. The blue curves are the result of the model. The black data points are the data. The raw OD600 data is reported in Table 7.10.

of succinate and glucose. OD and flux increase exponentially with rate equal to the initial steady state growth rate. Growth rate is constant in time and also equal to the steady state growth rate. During this time translational activity is constant at the steady state value of the initial culture. At about 0.1 OD600, glucose is exhausted and the exponential growth of OD600 is interrupted by a lag followed by a slower rate of increase. Protein synthesis flux decreases, deviating from its exponentially increasing behavior. The ribosomal protein mass does not significantly change during this time and the translational activity decreases along with flux.

Protein synthesis flux quickly begins increasing again as succinate flux takes over as the dominant carbon flux. The translational activity begins to increase as well, but is below the final steady state value. Thus the cell has a high catabolic protein synthesis rate and a small ribosomal protein synthesis rate, relative to the final steady state. Since the cell is able to invest a higher fraction of protein synthesis towards the flux-limiting catabolic proteins, flux transiently increases more quickly than the final steady state growth rate. As the stoichiometry of the flux producing catabolic enzymes and the flux consuming ribosomal proteins reaches the final steady state levels, the translational activity relaxes to its final steady state value and flux grows exponentially with the final steady state growth rate. Likewise, growth rate stabilizes at its constant final steady state value.

5.5   Acknowledgments

Chapter 6

Outlook

6.1   Lessons from this study

In this dissertation we are able to quantitatively predict the kinetics of bacterial mass accumulation throughout growth transitions using only observations from steady state growth and the known topology of regulatory interactions. The model does not include the complex molecular details of the underlying regulation. This demonstrates the power of this top-down physiological approach to describe bacterial physiology, even outside of steady state growth.

Our simple model provides a consistent framework that can reproduce some surprising observations of gene expression reported in the literature. We predict that if the initial nutrient flux is high enough just after upshift, the cell devotes a higher fraction of protein synthesis to ribosomes than it does in the final steady state. Schaechter and coworkers observed that for some nutrient upshifts of *Salmonella typhimurium* the RNA synthesis rate, which reflects the synthesis rate of ribosomes, is transiently higher than the rate in the final steady state condition [34]. We also predict that for these upshifts the cell expresses catabolic proteins at a rate lower than in the final steady state and can even completely suppress their expression transiently. This complete suppression of catabolic proteins was observed for carbon upshifts in *E. coli* in [14]. This coordinated regulation of the flux-producing catabolic enzymes and the flux-consuming ribosomes results in very fast relaxation of the fractional synthesis rate of ribosomal proteins. Indeed, the rate of synthesis of ribosomal protein normalized by the total protein synthesis rate in *E.*

coli increases from its initial value to its final value in just a few minutes after a carbon upshift [38] [39].

Our report provides new insights about the bacterial growth rate. In steady state growth, the growth rate quantifies the rate at which *all* cellular constituents increase and thus is the most basic quantity describing the state of the cell [3]. Remarkably, despite the immense complexity of the underlying regulatory networks, in steady state the growth rate is the primary determinant of the macromolecular composition of the bacterial cell [6] [9] [14]. However, throughout growth transitions, we find that while protein synthesis rates relax on a timescale of minutes, growth rate relaxes over the course of hours. Thus during excursions from steady state growth, even those as gentle as carbon upshift, the relationships between growth rate and macromolecular composition (or macromolecular synthesis rates) are not upheld. We predict that macromolecular synthesis rates are instead correlated with the translational activity. In this sense it may seem that the growth rate does not have the same importance as in steady state growth. We even find that in some situations the growth rate exceeds the steady state growth rate afforded by the medium for several hours, suggesting that in steady state the cell grows at a rate slower than it is capable of. However, the growth rate of the final condition is still a measure of the quality of the new growth condition and manifests itself well before the final growth rate is reached (*e.g.* as the rate of increase of protein synthesis rate).

Our study also suggests a tradeoff between the steady state growth rate and the ability of the bacterial cell to adjust to changing growth conditions. In our model the translational activity adapts to balance flux throughout carbon upshift. At slower growth the translational activity is especially low because the ribosome amount is nonzero at zero growth rate and there are many more ribosomes than necessary to keep up with the protein synthesis rate. This facilitates faster carbon upshift since the activity of ribosomes can easily increase in response to increased substrate concentration. However, it means that more ribosomes are produced than are necessary for the required protein synthesis in steady state. The extra ribosomes can be considered unnecessary protein and come at the expense of the steady state growth rate as described in [9].

6.2 Remaining questions and future directions

We have predicted the kinetics of protein mass accumulation throughout carbon upshift and downshift. To get a deeper physiological understanding we plan to extend the presented study. Our model also predicts the expression of ribosomal proteins without any additional fit parameters. Measuring ribosome expression will provide a deeper exploration of the quantitative predictions of the model. Although the measurement of OD600 throughout these growth transitions allows for high temporal precision, we also plan to directly measure total protein amount to avoid effects related to cell size and other factors influencing spectrometry. Combining the observations of total protein and ribosome amount will also provide a direct measure of the translational activity, which is central to our understanding.

In our model we are able to avoid explicitly keeping track of the kinetics of regulatory metabolites because we have a handle on the translational activity, which is also determined by the metabolites. As a result we developed a model that captures the kinetics of mass accumulation throughout carbon upshift that is simple and analytically solvable with only a single unknown parameter. The effectiveness of our approach warrants exploring its usefulness in the study of other complex or poorly characterized systems. In particular other types of bacterial growth transitions may benefit from our approach. Nitrogen, phosphate, osmolarity, antibiotics, temperature and many other changing conditions may benefit from similar phenomenological models.

Within the context of carbon shifts there are still remaining questions about the fluxes of other nutrients. For the shifts we studied we did not need to explicitly consider that other nutrients (*e.g.* nitrogen) may be limiting. More extreme upshifts would likely require such considerations and would provide insight about the regulation of the limiting enzymes.

In our study we also discovered that too much carbon flux inhibits growth (data not shown). Adding lactose, succinate, or glycerol to cultures that have a high expression of the relevant catabolic enzymes (*i.e.* the *lac*, *dctA*, and *glp* operons) was found to inhibit growth rather than facilitate it. The mechanism of these growth inhibitions is not fully understood and it will be interesting to explore this further.

The cell produces the enzymes responsible for the metabolism of some carbon

sources before they are present in the medium and are thus immediately able to utilize these carbon sources at the instant they are added to the medium [14] [40]. Production of these proteins is useless in the absence of their substrates and is a waste of cellular resources that results in a decrease in the growth rate. The observation that this is true for different carbon sources to varying degrees suggests that the cell is programmed to expect the appearance of particular carbon sources over others. Careful quantitative study of the upshift kinetics of various carbon sources may provide insight about the natural environment of *E. coli*.

6.3   Acknowledgments

With permission from the coauthors, all chapters of this dissertation contain work from a manuscript that is in preparation with the working title "A quantitative theory for the kinetics of bacterial growth transition" 2014, D. W. Erickson, S. Schink, U. Gerland, and T. Hwa.

Chapter 7

Additional information

7.1 Experimental procedures

Growth medium: All growth media used in this study were based on N^-C^- minimal medium [41], which contains K_2SO_4 (1 g), $K_2HPO_4·3H_2O$ (17.7 g), KH_2PO_4 (4.7 g), $MgSO_4·7H_2O$ (0.1 g), and NaCl (2.5 g) in one liter, and is supplemented with 20 mM NH_4Cl and various carbon sources. IPTG was added to media when necessary to fully induce the native lacZ operon or $P_{Llac-O1}$ promoter driving XylR.

Growth: Each experiment was carried out in three steps: seed culture in LB broth, pre-culture and experimental culture in identical N^-C^- minimal medium. For seed culture, one colony from fresh LB agar plate was inoculated into liquid LB and cultured at 37°C with shaking. Then depending on the specific growth rate in each condition, cells in various cultures were diluted to different densities in identical N^-C^- minimal medium, and cultured in 37°C shaking at 250rpm overnight (pre-culture), so that the overnight culture was kept in exponential growth for at least 3 doublings. Cells from the overnight pre-culture was then diluted to OD600 = 0.005-0.04 in identical pre-warmed minimal medium, and cultured in 37°C shaking at 250rpm (experimental culture).

Batch culture growth: All batch culture growth was performed in a 37°C water bath shaker shaking at 250 rpm. The culture volume was either 5 ml in 20 mm × 150 mm test tubes or 25 ml in 125 ml flasks. Throughout growth, 200 μl cell culture was collected in a Sterna Sub-Micro Cuvette for OD600 measurement using a ThermoScientific Genesys 20 Spectrophotometer.

Flowcell culture growth: All flowcell culture growth was performed in a 37°C air incubator. The culture volume was 25 ml in 125 ml flasks and was kept shaking at 250 rpm. A peristaltic pump was used to circulate the culture through a flowcell cuvette and back to the flask. OD600 was measured once per second using a ThermoScientific Genesys 20 Spectrophotometer connected to a computer with a serial cable. The pump was cycled between on and off states (typically 25 seconds on and 15 seconds off) because the OD600 data was found to have much more uncertainty while the pump was on.

Strains: The strains used in this study are derived from *E. coli* K12 strain NCM3722 [42] [43] and are summarized in Table 7.1.

Chromosomal Pu-*dctA* fusion: Because the activation of Pu promoter needs the XylR protein, we started with the strain NQ386 (from [14]) in which a synthetic *lacZ* promoter $P_{Llac-O1}$ [44] (a promoter that is repressed by LacI but does not need Crp-cAMP for activation) drives *xylR* at the *attB* site. A DNA fragment containing the *Pu* promoter (-1 bp to -178 bp relative to the transcriptional start site) was amplified by PCR from a *Pu* promoter containing plasmid pEZ9 [36], then inserted into the SalI and BamHI sites of plasmid pKD13, producing plasmid pKDPu. Using this plasmid as a template, the region containing the *km* gene and *Pu* promoter was PCR amplified and integrated into the chromosome of *E. coli* strain NQ351 in front of *dctA* (-1 to -182bp relative to translational start site) by using the λ Red system [45]. The *km*-Pu-*dctA* construct in NQ351 was transferred into strain NQ386 containing $P_{Llac-O1}$ by P1 transduction, resulting in strain NQ530.

β-galactosidase assay: Samples (0.5mL culture) were collected during growth. LacZ assay samples were immediately added to an equal volume of the freshly prepared Z-buffer (in 1 L: 8.52 g Na_2HPO_4, 5.5 g $NaH_2PO_4 \cdot H_2O$, 0.75 g KCl and 0.25 g $MgSO_4 \cdot 7H_2O$, pH adjusted to 7.0; with 0.004% (w/v) SDS and 40 mM β-mercaptoethanol) with 100 μl chloroform. Cells were immediately disrupted by vortexing. After all the samples were collected, they were briefly vortexed a second time. After 5-10 minutes at room temperature to settle the chloroform, the lysates were optionally diluted (typically 1:20) into 50:50 mixture of Z-Buffer and media. 200 μL was then added to a 96-well plate. Immediately prior to reading in GENiosPro (Tecan) plate reader, 40 μl of 4 mg/mL ortho-Nitrophenyl-β-galactoside in 0.1 M phosphate

buffer (pH=7.0) was added to each well. The plate reader was set to read absorbance at a wavelength of 420 nm every minute for 60 to 120 minutes at 28°C.

7.2   Tables

Table 7.1: Strains used in this study.

Strain	Genotype	Description
NCM3722	wild-type *E. coli* K12 strain	parent strain for all strains used here
NQ354	$\Delta lacI$	*laci*-null
NQ530	$attB$::P$_{\text{Llac-O1}}$-xylR, P$dctA$::km-Pu	titratable DctA
NQ351	pKD46	NCM3722 with pKD46 plasmid
NQ386	$attB$::P$_{\text{Llac-O1}}$-xylR	*xylR* expression strain

Table 7.2: Parameter values used in the model. The model requires the knowledge of three parameters obtained from the steady state growth relationships. Here we report the values used, which were obtained from a best fit.

Parameter	Value
$\phi_{R,min}$	0.0714
γ_{max}	$4.65\,\text{h}^{-1}$
λ_C	$1.2\,\text{h}^{-1}$

Table 7.3: Glucose-glycerol diauxie data. Wild-type *E. coli* NCM3722 is grown at 37°C in minimal medium with glucose and glycerol. These data are plotted in Figure 1.3

Time (h)	OD600
-1.6333	0.076
-1.2167	0.112
-0.88333	0.155
-0.61667	0.199
-0.41667	0.241
-0.26667	0.277
-0.16667	0.303
-0.1	0.323
0	0.353
0.1	0.36
0.21667	0.359
0.35	0.357
0.48333	0.362
0.61667	0.372
0.75	0.392
0.86667	0.419
1	0.45
1.1167	0.492
1.2333	0.536
1.3333	0.582
1.4667	0.64
1.6333	0.714
1.8167	0.807

Table 7.4: Long time batch culture data for the succinate add gluconate upshift. Wild-type NCM3722 cells were grown in minimal medium at 37°C with 1 mM IPTG and 0.4% succinate as the sole carbon source. At time zero gluconate was added to a final concentration of 20 mM. Culture saturation was avoided by serial dilution into a fresh, identical culture. The OD600 data for the 3 overlapping cultures is reported here.

Culture1		Culture2		Culture3	
Time after upshift (h)	OD600	Time after upshift (h)	OD600	Time after upshift (h)	OD600
-2.48	0.035	1.32	0.058	3.07	0.06
-2.1	0.043	1.65	0.077	3.4	0.081
-1.75	0.048	1.98	0.101	3.73	0.107
-1.43	0.054	2.32	0.135	4.07	0.147
-1.1	0.063	2.65	0.182	4.4	0.199
-0.77	0.073	2.98	0.247	4.73	0.272
-0.43	0.084	3.32	0.331	0	0
-0.1	0.098				
0.07	0.101				
0.23	0.111				
0.4	0.127				
0.57	0.137				
0.9	0.173				
1.23	0.222				
1.57	0.288				
1.9	0.375				

Table 7.5: LacZ throughout the mannose add lactose upshift. Wild-type NCM3722 cells were grown in 0.4% mannose. At time zero, 0.4% lactose was added. LacZ was measured using an activity assay.

Time after up-shift (h)	LacZ activity (U/mL)
0	14.4396
0.033333	13.1519
0.066667	12.7725
0.1	21.2493
0.13333	34.2047
0.18333	60.5316
0.21667	58.2895
0.25	65.014
0.28333	81.2374
0.31667	86.8812
0.35	105.487
0.38333	103.918
0.41667	110.134
0.45	114.594
0.48333	130.426
0.56667	142.025
0.65	119.703
0.81667	163.684
0.98333	225.435
1.25	352.007
1.4333	479.576
1.5	453.6248
1.7333	548.439
1.9	788.2434

Table 7.6: Mannose add succinate LacZ. NQ354 ($\Delta lacI$) cells were grown in 0.1% mannose. At time zero, 0.4% succinate was added. Here we report the LacZ activity.

Time after up-shift (h)	LacZ activity (U/mL)	Time after up-shift continued (h)	LacZ activity continued (U/mL)
-1.9583	2580.21	0.475	3969.75
-1.025	3192.26	0.525	4078.93
-0.85833	3031.33	0.60833	3902.23
-0.69167	3191.98	0.69167	4065.72
-0.525	3192.82	0.775	4254.39
-0.35833	3340.74	0.85833	4285.28
-0.19167	3336.92	0.94167	4649.34
-0.025	3586.27	1.025	4546.31
0.0083333	3785.93	1.1083	4564.47
0.041667	3709.75	1.1917	4586.45
0.075	3598.63	1.275	4838.76
0.10833	3735.86	1.375	4914.16
0.14167	3368.36	1.4417	5265.28
0.175	3823.08	1.525	5370.65
0.225	3764.28	1.6083	5371.35
0.275	3749.86	1.6583	5644.11
0.325	3803.73	1.6917	5396.67
0.375	3762.25	1.725	5829.98
0.425	3886.25	1.7583	5798.18

Table 7.7: Upshift with direct titration of the initial carbon flux. NQ530 cells were grown in 0.1%mannose with 100 μM IPTG and 0, 32, or 64 μM 3MBA, as labeled in this table. At time zero succinate is added to 20 mM and 3MBA is added to 64 μM. Here we report the raw OD600 data.

Time after upshift (h)	0 μM	32 μM	64μM
-2.6917	0.042	0.041	0.039
-2.325	0.047	0.046	0.044
-1.325	0.06	0.057	0.056
-0.79167	0.069	0.067	0.065
-0.0083333	0.084	0.08	0.076
0.15833	0.084	0.081	0.076
0.325	0.089	0.09	0.081
0.475	0.093	0.096	0.089
0.625	0.099	0.104	0.098
0.775	0.106	0.115	0.111
0.925	0.114	0.12	0.12
1.075	0.122	0.13	0.131
1.225	0.13	0.138	0.143
1.375	0.138	0.148	0.156
1.525	0.147	0.157	0.171
1.675	0.157	0.169	0.188
1.825	0.171	0.183	0.203
1.975	0.179	0.196	0.221
2.125	0.19	0.209	0.241
2.275	0.205	0.225	0.261
2.425	0.216	0.241	0.282
2.575	0.24	0.259	0.299
2.725	0.248	0.278	0.317
2.875	0.265	0.296	0.343
3.025	0.284	0.317	0.367
Continued on next page			

Table 7.7: Upshift with direct titration of the initial carbon flux, Continued.

Time after upshift (h)	0 µM	32 µM	64µM
3.175	0.303	0.341	0.397
3.325	0.326	0.364	0.428
3.475	0.345	0.389	0.455
3.625	0.368	0.418	0.488

Table 7.8: Pyruvate with gluconate depletion data. Wild-type NCM3722 cells were grown in the presence of 1mM IPTG. The only carbon sources are 20mM pyruvate and 5.6mM gluconate. The raw OD600 data is reported here.

Time (h)	OD600
1.03	0.04
1.23	0.05
1.45	0.061
1.67	0.076
1.83	0.091
2	0.106
2.17	0.125
2.33	0.147
2.5	0.159
2.67	0.17
2.83	0.185
3	0.201
3.17	0.225
3.33	0.253
3.5	0.285
3.75	0.339
4	0.401
4.25	0.472
4.5	0.555

Table 7.9: Succinate with gluconate depletion data. Wild-type NCM3722 cells were grown in the presence of 1mM IPTG with 20mM succinate and 5.6mM gluconate as carbon sources. The raw OD600 data is reported here.

Time (h)	OD600
1.03	0.038
1.23	0.045
1.45	0.055
1.67	0.067
1.83	0.078
2	0.09
2.17	0.101
2.33	0.11
2.5	0.117
2.67	0.124
2.83	0.131
3	0.138
3.17	0.146
3.33	0.155
3.5	0.165
3.75	0.183
4	0.205
4.25	0.227
4.5	0.25
4.83	0.282
5.17	0.322
5.5	0.367

Table 7.10: Succinate with glucose depletion data. Wild-type NCM3722 cells were grown on 0.4% succinate and 0.5mM glucose as the only carbon sources. The raw OD600 data is reported here.

Time (h)	OD600
1.03	0.036
1.23	0.043
1.45	0.053
1.67	0.065
1.83	0.076
2	0.089
2.17	0.103
2.33	0.113
2.5	0.117
2.67	0.121
2.83	0.126
3	0.132
3.17	0.138
3.33	0.145
3.5	0.15
3.75	0.159
4	0.172
4.25	0.189
4.5	0.205
4.83	0.23
5.17	0.257
5.5	0.293
5.83	0.328

7.3 Acknowledgments

Bibliography

[1] Whitney Hollinshead, Lian He, and Yinjie J Tang. Biofuel production: an odyssey from metabolic engineering to fermentation scale-up. *Front Microbiol*, 5:344, Jan 2014.

[2] Måns Ehrenberg, Hans Bremer, and Patrick P Dennis. Medium-dependent control of the bacterial growth rate. *Biochimie*, 95(4):643–58, Apr 2013.

[3] A Campbell. Synchronization of cell division. *Bacteriol Rev*, 21(4):263–72, Dec 1957.

[4] Moselio Schaechter. From growth physiology to systems biology. *Int Microbiol*, 9(3):157–61, Sep 2006.

[5] Jacques Monod. The growth of bacterial cultures. *Annual Reviews in Microbiology*, Jan 1949.

[6] Moselio Schaechter, O Maaløe, and N O Kjeldgaard. Dependency on medium and temperature of cell size and chemical composition during balanced grown of salmonella typhimurium. *J Gen Microbiol*, 19(3):592–606, Dec 1958.

[7] S Cooper. The origins and meaning of the schaechter-maaløe-kjeldgaard experiments. *Journal of General Microbiology*, Jan 1993.

[8] Frederick C Neidhardt. Bacterial growth: constant obsession with dn/dt. *J Bacteriol*, 181(24):7405–8, Dec 1999.

[9] Matthew Scott, Carl W Gunderson, Eduard M Mateescu, Zhongge Zhang, and Terence Hwa. Interdependence of cell growth and gene expression: origins and consequences. *Science*, 330(6007):1099–102, Nov 2010.

[10] J R Warner. The economics of ribosome biosynthesis in yeast. *Trends Biochem Sci*, 24(11):437–40, Nov 1999.

[11] H Bremer and P Dennis. Modulation of chemical composition and other parameters of the cell by growth rate. *Escherichia coli and Salmonella: cellular . . .*, Jan 1996.

[12] Frederick C Neidhardt and B Magasanik. Studies on the role of ribonucleic acid in the growth of bacteria. *Biochim Biophys Acta*, 42:99–116, Jul 1960.

[13] J Forchhammer and L Lindahl. Growth rate of polypeptide chains as a function of the cell growth rate in a mutant of escherichia coli 15. *J Mol Biol*, 55(3):563–8, Feb 1971.

[14] Conghui You, Hiroyuki Okano, Sheng Hui, Zhongge Zhang, Minsu Kim, Carl W Gunderson, Yi-Ping Wang, Peter Lenz, Dalai Yan, and Terence Hwa. Coordination of bacterial proteome with metabolism by cyclic amp signalling. *Nature*, pages 1–6, Aug 2013.

[15] D G Dalbow and R Young. Synthesis time of beta-galactosidase in escherichia coli b/r as a function of growth rate. *Biochem J*, 150(1):13–20, Jul 1975.

[16] R Young and Hans Bremer. Polypeptide-chain-elongation rate in escherichia coli b/r as a function of growth rate. *Biochem J*, 160(2):185–94, Nov 1976.

[17] S Pedersen. Escherichia coli ribosomes translate in vivo with variable rate. *The EMBO Journal*, 3(12):2895–8, Dec 1984.

[18] Stefan Klumpp, Matthew Scott, Steen Pedersen, and Terence Hwa. Molecular crowding limits translation and cell growth. *Proc Natl Acad Sci USA*, Sep 2013.

[19] J L Botsford and J G Harman. Cyclic amp in prokaryotes. *Microbiol Rev*, 56(1):100–22, Mar 1992.

[20] A Kolb, S Busby, H Buc, S Garges, and Sankar Adhya. Transcriptional regulation by camp and its receptor protein. *Annu Rev Biochem*, 62:749–95, Jan 1993.

[21] M H Saier, B U Feucht, and L J Hofstadter. Regulation of carbohydrate uptake and adenylate cyclase activity mediated by the enzymes ii of the phosphoenolpyruvate: sugar phosphotransferase system in escherichia coli. *J Biol Chem*, 251(3):883–92, Feb 1976.

[22] Josef Deutscher, Christof Francke, and Pieter W Postma. How phosphotransferase system-related protein phosphorylation regulates carbohydrate metabolism in bacteria. *Microbiol Mol Biol Rev*, 70(4):939–1031, Dec 2006.

[23] W Epstein, L B Rothman-Denes, and J Hesse. Adenosine 3':5'-cyclic monophosphate as mediator of catabolite repression in escherichia coli. *Proc Natl Acad Sci USA*, 72(6):2300–4, Jun 1975.

[24] B M Hogema, J C Arents, T Inada, H Aiba, K van Dam, and P W Postma. Catabolite repression by glucose 6-phosphate, gluconate and lactose in escherichia coli. *Mol Microbiol*, 24(4):857–67, May 1997.

[25] Katja Bettenbrock, Thomas Sauter, Knut Jahreis, Andreas Kremling, Joseph W Lengeler, and Ernst-Dieter Gilles. Correlation between growth rates, eiiacrr phosphorylation, and intracellular cyclic amp levels in escherichia coli k-12. *J Bacteriol*, 189(19):6891–900, Oct 2007.

[26] Thomas Kuhlman, Zhongge Zhang, Milton H Saier, and Terence Hwa. Combinatorial transcriptional control of the lactose operon of escherichia coli. *Proc Natl Acad Sci USA*, 104(14):6043–8, Apr 2007.

[27] Markus Basan, Sheng Hui, Zhongge Zhang, Yang Shen, James R Williamson, and Terence Hwa. Efficient allocation of proteomic resources for energy metabolism results in acetate overflow. In submission, 2014.

[28] Rutger Hermsen, Hiroyuki Okano, Conghui You, Nicole Werner, and Terence Hwa. A growth-rate composition formula for the growth of bacteria on mixed substrates. In submission, 2014.

[29] Jacques Monod. Recherche sur la croissance des cultures bacteriennes. *Hermann et Cie, Paris, France.*, pages 1–106, Oct 1942.

[30] Jacques Monod. The phenomenon of enzymatic adaptation - and its bearings on problems of genetics and cellular differentiation, Jan 1947.

[31] Hans Bremer and P P Dennis. Transition period following a nutritional shift-up in the bacterium escherichia coli b/r: stable rna and protein synthesis. *J Theor Biol*, 52(2):365–82, Aug 1975.

[32] Patrick P Dennis, Mans Ehrenberg, and Hans Bremer. Control of rrna synthesis in escherichia coli: a systems biology approach. *Microbiol Mol Biol Rev*, 68(4):639–68, Dec 2004.

[33] Steven Strogatz. *Nonlinear dynamics and chaos: with applications to physics, biology and chemistry.* 2001.

[34] N O Kjeldgaard, O Maaløe, and Moselio Schaechter. The transition between different physiological states during balanced growth of salmonella typhimurium. *J Gen Microbiol*, 19(3):607–16, Dec 1958.

[35] Sidhartha Goyal, Jie Yuan, Thomas Chen, Joshua D Rabinowitz, and Ned S Wingreen. Achieving optimal growth through product feedback inhibition in metabolism. *PLoS Comput Biol*, 6(6):e1000802, Jun 2010.

[36] V de Lorenzo, M Herrero, M Metzke, and K N Timmis. An upstream xylr- and ihf-induced nucleoprotein complex regulates the sigma 54-dependent pu promoter of tol plasmid. *The EMBO Journal*, 10(5):1159–67, May 1991.

[37] Agata M Pudlik and Juke S Lolkema. Mechanism of citrate metabolism by an oxaloacetate decarboxylase-deficient mutant of lactococcus lactis il1403. *J Bacteriol*, 193(16):4049–56, Aug 2011.

[38] R Schleif. Control of production of ribosomal protein. *J Mol Biol*, 27(1):41–55, Jul 1967.

[39] P P Dennis and Hans Bremer. Letters to the editor: Regulation of ribonucleic acid synthesis in escherichia coli b/r: an analysis of a shift-up. iii. stable rna synthesis rate and ribosomal rna chain growth rate following a shift-up. *J Mol Biol*, 89(1):233–239, Oct 1974.

[40] H L Kornberg and R E Reeves. Inducible phosphoenolpyruvate-dependent hexose phosphotransferase activities in escherichia coli. *Biochem J*, 128(5):1339–44, Aug 1972.

[41] L N Csonka, T P Ikeda, S A Fletcher, and S Kustu. The accumulation of glutamate is necessary for optimal growth of salmonella typhimurium in media of high osmolality but not induction of the prou operon. *J Bacteriol*, 176(20):6324–33, Oct 1994.

[42] Eric Soupene, Wally C van Heeswijk, Jacqueline Plumbridge, Valley Stewart, Daniel Bertenthal, Haidy Lee, Gyaneshwar Prasad, Oleg Paliy, Parinya Charernnoppakul, and Sydney Kustu. Physiological studies of escherichia coli strain mg1655: growth defects and apparent cross-regulation of gene expression. *J Bacteriol*, 185(18):5611–26, Sep 2003.

[43] Eric Lyons, Michael Freeling, Sydney Kustu, and William Inwood. Using genomic sequencing for classical genetics in e. coli k12. *PLoS ONE*, 6(2):e16717, Jan 2011.

[44] R Lutz and H Bujard. Independent and tight regulation of transcriptional units in escherichia coli via the lacr/o, the tetr/o and arac/i1-i2 regulatory elements. *Nucleic acids research*, 25(6):1203–10, Mar 1997.

[45] K A Datsenko and B L Wanner. One-step inactivation of chromosomal genes in escherichia coli k-12 using pcr products. *Proc Natl Acad Sci USA*, 97(12):6640–5, Jun 2000.